Important Notice

UNIVERSITY OF CALGARY

A comparison of different methods for estimating Thomsen's anisotropy parameters

by

Chunyan Xiao

A THESIS

SUBMITTED TO THE FACULTY OF GRADUATE STUDIES

IN PARTIAL FULFILMENT OF THE REQUIREMENTS FOR THE

DEGREE OF MASTER OF SCIENCE

DEPARTMENT OF GEOLOGY AND GEOPHYSICS

CALGARY, ALBERTA

SEPTEMPER, 2006

UNIVERSITY OF CALGARY

FACULTY OF GRADUATE STUDIES

The undersigned certify that they have read, and recommend to the Faculty of Graduate Studies for acceptance, a thesis entitled "A comparison of different methods for estimating Thomsen anisotropy parameters" submitted by Chunyan Xiao in partial fulfilment of the requirements of the degree of Master of Science.

Supervisor, Dr. John Bancroft, Geology and Geophysics

Dr. Larry R. Lines, Geology and Geophysics

External Examiner, Dr. J.A.R. Blais, Geomatics Engineering

22 September 2006

Abstract

Various anisotropic moveout velocity analysis methods are used to estimate anisotropy parameters in a VTI medium in combination with well-log data. Analyses of four reflection-traveltime inversions in weakly anisotropic media show that inversion accuracy is related to spread length and subsurface anisotropy parameters. Within its own offset range (hyperbolic, shifted hyperbolic, modified three-term Taylor series or Alkhalifah's), the accuracy of estimated δ decreases with offset and the accuracy of estimated ε increases with offset. The smaller the value of $(\varepsilon - \delta)$, the greater the accuracy of the estimated δ value. The results from the four reflection-traveltime inversions by semblance analysis for synthetic seismic examples demonstrate that in estimating δ, the Alkhalifah's and the shifted hyperbolic estimations are better than the modified three-term Taylor-series method. Only the Alkhalifah's approximation can be used to estimate the anisotropy parameter ε accurately. Hyperbolic estimation is only suitable for estimation of elliptical anisotropy.

Anisotropy parameters were obtained by anisotropic moveout velocity analysis performed on Blackfoot P-wave reflection-seismic data, in combination with sonic-log data. The results show that estimated values of ε and δ seem reasonable only if the time intervals of the layer are larger than about 200 ms. When the lower three layers are combined as one target layer, it exhibits relatively high values of ε and δ.

Acknowledgements

I would like to extend my gratitude to the many people that I have worked with and who have helped to make this thesis possible over the last couple of years. The greatest acknowledgement goes to my supervisor, John Bancroft, and to Jim Brown, who encouraged and guided me through all my work at the University of Calgary and greatly enhanced the results presented as part of this thesis.

Special thanks are given to Drs. Larry Lines, Don Lawton, Gary Margrave, E.S. Krebes, Robert Stewart, and Helen Isaac for their academic instruction. I also thank Hanxing Lu for processing and ProMAX help over the last two years. I am grateful to Kevin Hall and Chuck Ursenbach for their assistance. Special thanks to Mark Kirtland, who proofread and edited this thesis for English usage. I would like to thank Zhihong Cao, Xiang Du, Lingping Dong, and Richard Xu, who were always available to help out.

I gratefully acknowledge CREWES sponsors for providing me with financial support during my studies. I would like to thank all of the students, staff and professors at the University of Calgary for their assistance and friendship.

Finally, I thank Donghai, my husband, and Xiaoyue, my lovely daughter, for their sacrifice of time and love.

Dedication

To My Father

In Memoriam

Table of Contents

Approval Page ii
Abstract iii
Acknowledgements iv
Dedication v
Table of Contents vi
List of Tables viii
List of Figures and Illustrations ix
List of Symbols, Abbreviations and Nomenclature xii

CHAPTER 1: INTRODUCTION 1
1.1. Motivation 1
1.2. Organization of the thesis 6
1.3. Contribution of the thesis 7

CHAPTER 2: DIFFERENT METHODS FOR ESTIMATING THOMSEN'S ANISOTROPY PARAMETERS(LITERATURE REVIEW) 10
2.1. Phase slowness methods 10
2.2. Direct traveltime inversion methods 13
2.3. $\tau - p$ methods 15
2.4. DMO inversion methods 20
2.5. Anisotropy moveout velocity analysis methods 24
2.6. An initial comparison of different methods 26
2.6.1 A comparison of hyperbolic moveout velocity analysis, phase slowness and direct traveltime inversion methods 27
2.6.2 A comparison of the modified three-term Taylor series, shifted hyperbolic and $\tau - p$ methods 29
2.6.3 A comparison of DMO inversion and Alkhalifah's inversion methods 32

CHAPTER 3: ANISOTROPIC MOVEOUT VELOCITY ANALYSIS METHODS FOR ESTIMATING THOMSEN'S ANISOTROPY PARAMETERS FROM P-WAVE MOVEOUT IN VTI LAYERS 34
3.1 Formulations for estimations of Thomsen's anisotropy parameters in layered anisotropic media 35
3.1.1 Hyperbolic estimates 35
3.1.2 Shifted hyperbolic estimates 37
3.1.3 Modified three-term Taylor series estimates 39
3.1.4 Alkhalifah's estimates 45
3.1.5 Estimates in multilayered media 46
3.2 Reflection-traveltime approximations of four moveout equations to true traveltime in layered anisotropic media 49
3.2.1 Approximations versus offset range 52
3.2.2 Approximations versus anisotropy parameters 53
3.2.3 Approximations versus vertical P-wave velocity 55

3.2.4 Approximations versus zero-offset traveltime....56
3.3 Approaches for estimating effective parameters in layered anisotropic media....57
3.3.1 Procedure for estimating Thomsen's anisotropy parameters....57
3.3.2 Mean-square traveltime fitting....58
3.3.3 Semblance analysis....59

CHAPTER 4: SYNTHETIC INVERSIONS OF P-WAVE MOVEOUTS IN VTI LAYERS....62
4.1. Single VTI layer over an isotropic layer....62
4.1.1 Estimation of Thomsen's anisotropy parameters versus offset range....64
4.1.2 Estimation of Thomsen's anisotropy parameters versus model anisotropy parameters....65
4.2. Layered VTI media....67
4.3. Conclusions....68

CHAPTER 5: APPLICATION TO BLACKFOOT SEISMIC DATA....70
5.1. Blackfoot seismic data processing....70
5.2. Interval vertical velocities from sonic log....75
5.3. Estimation of Thomsen's anisotropy parameters....76
5.4. Interpretation and discussion....78

CHAPTER 6: CONCLUSIONS....79

REFERENCES....81

APPENDIX A: SHIFTED HYPERBOLA MOVEOUT EQUATIONS....87

List of Tables

Table 2.1 A comparison of hyperbolic moveout velocity analysis, phase slowness and direct traveltime inversion methods....29

Table 2.2 A comparison of the modified three-term Taylor series, shifted hyperbolic and $\tau - p$ methods....32

Table 2.3 A comparison of DMO inversion and Alkhalifah's inversion methods. 33

Table 4.1 Model parameters for layered VTI media 67

Table 4.2 The methods for estimating anisotropy parameters and their evaluation of estimated anisotropy parameters at short and long offsets 69

Table 5.1 Estimated effective coefficients and anisotropy parameters (time interval < 200 ms) 77

Table 5.2 Estimated effective coefficients and anisotropy parameters (time interval > 200 ms) 77

List of Figures and Illustrations

Figure 1.1 P wavefronts vary with anisotropy parameters ε and δ: (a) the values of ε are fixed at 0.2, and those of δ range from –0.6 to 1.0 in increments of 0.2. (b) the values of δ are fixed at 0.2, and those of ε range from –0.6 to 1.0 in increments of 0.2. (After John Bancroft, private communication).....3

Figure 2.1 Vertical slowness at depth. (a) Synthetic P-wave offset VSP illustrating vertical slowness estimate $\Delta t / \Delta z$. (b) The model consists of receiver depths ranging from 213.36 to 670.56 m at 15.24 m intervals and source offsets of 457.2 m. (After Gaiser, 1990).....12

Figure 2.2 Horizontal slowness at surface. (a) Synthetic P-wave offset VSP illustrating horizontal slowness estimate $\Delta t / \Delta x$. (b) The model consists of receiver depths from 487.68 m and source offsets ranging from 30.48 to 914.4 m at 30.48 m intervals. (After Gaiser, 1990).....12

Figure 2.3 Description of the field experiment for a given location of the source. (After White et al., 1983).....13

Figure 2.4 The two-layer model. *H* denotes top layer thickness. *Z* gives the depth of the receiver in the buried layer. The horizontal source-receiver offset is denoted as *X*. The symbol *r* corresponds to the lateral distance between the receiver and the refraction point. (After Brown et al., 2000).....14

Figure 2.5 SV-wave moveout curve with a cusp. Model parameters are (from Thomsen, 1986): $\alpha_0 = 3.048$ km/s, $\beta_0 = 1.490$ km/s, $\varepsilon = 0.255$, $\delta = -0.05$ ($\sigma = 1.276$), $z = 3$ km. (After Tsvankin and Thomsen, 1994).....16

Figure 2.6 Layer stripping in the $\tau - p$ domain: (a) $\tau - p_x$ curves; (b) first layer removed; (c) top two layers removed. (After Baan and Kendall, 2002).....19

Figure 3.1 Wavefronts on a depth section for varying anisotropy values, a) ε = 0.2 with varying δ = -0.6 to 0.6, and (b) δ = -0.2 with varying ε = -0.4 to 0.6.....35

Figure 3.2 SV-wave moveout with negative σ for the model of Mesaverde mudshale from Levin (1989): $\alpha_0 = 4.529$ km/s, $\beta_0 = 2.703$ km/s, $\varepsilon = 0.034$, $\delta = 0.211$ ($\sigma = -0.497$, $1 + 2\sigma = 0.006$), $z = 3$ km. (After Tsvankin and Thomsen, 1994).....36

Figure 3.3 Geometry of a hyperbolic NMO equation and the shifted hyperbola NMO equation. (After John Bancroft, private communication).....38

Figure 3.4 Maximum differences between the exact traveltimes and the best-fit hyperbola as a function of spread-length-to-depth ratio x_{max}/z. The model is Taylor sandstone with $z = 3$ km. (After Tsvankin and Thomsen, 1994).....40

Figure 3.5 Three term Taylor series t_T and approximation t_A for P-wave moveout in a layer of Dog Creek shale with z=3 km. (After Tsvankin and Thomsen, 1994).....44

Figure 3.6 Three term Taylor series t_T and approximation t_A for SV-wave moveout in a layer of Dog Creek shale with $z = 3$ km. (After Tsvankin and Thomsen, 1994).....45

Figure 3.7 Reflection-traveltime approximations to true reflection traveltime under different offset ranges. Blue line: the exact traveltime; purple line: hyperbolic approximation; green line: the modified three-term Taylor-series approximation; red line: the shifted-hyperbolic approximation; cyan line: Alkhalifah's approximation. 53

Figure 3.8 Reflection-traveltime approximations to true reflection traveltime under different anisotropy parameters. Solid blue line: the exact traveltime; purple dotted line: hyperbolic approximation; green dash-dot line: the modified three-term Taylor-series approximation; red solid line: the shifted-hyperbolic approximation; cyan dashed line: Alkhalifah's approximation. 54

Figure 3.9 Reflection-traveltime approximations to true reflection traveltime under different vertical velocities. Solid blue line: the exact traveltime; purple dotted line: hyperbolic approximation; green dash-dot line: the modified three-term Taylor-series approximation; red solid line: the shifted-hyperbolic approximation; cyan dashed line: Alkhalifah's approximation. 55

Figure 3.10 Reflection-traveltime approximations to true reflection traveltime under different zero-offset two-way traveltime. Solid blue line: the exact traveltime; purple dotted line: hyperbolic approximation; green dash-dot line: the modified three-term Taylor-series approximation; red solid line: the shifted-hyperbolic approximation; cyan dashed line: Alkhalifah's approximation. 56

Figure 3.11 The semblance plots using Alkhalifah's approximation for parameters: $\varepsilon = 0.2$, $\delta = -0.2$ with (a) Δt_{rms} contour; (b) traveltime versus offset. 59

Figure 3.12 The semblance plots using Alkhalifah's approximation for anisotropy parameters: (a) $\varepsilon = 0.2$, $\delta = 0.2$; (b) $\varepsilon = 0.2$, $\delta = 0.1$; (c) $\varepsilon = 0.2$, $\delta = -0.2$. 61

Figure 4.1 Model parameters 62

Figure 4.2 This figure indicates the noncorrelation of the two anisotropy parameters δ and ε for the measured anisotropy in sedimentary rocks. (Thomson, 1986) 63

Figure 4.3 Reflection-traveltime approximations to true reflection traveltime within different offset ranges. 64

Figure 4.4 The error in estimated δ plotted vs. true δ for various values of ε, for offset/depth = 1.0. Blue solid line: the exact anisotropy parameters; purple dotted line: hyperbolic traveltime inversion; green dash-dot line: the modified three-term Taylor-series inversion; red solid line: the shifted hyperbolic inversion; cyan dashed line: Alkhalifah's inversion. 65

Figure 4.5 The error in estimated ε plotted vs. true δ when offset/depth = 2.0. Green dash-dot line: the modified three-term Taylor-series inversion; red solid line: the shifted hyperbolic inversion; cyan dashed line: Alkhalifah's inversion. 66

Figure 5.1 Post-stack migration using a sequence of conventional algorithms. 73

Figure 5.2 Correlation of synthetic data and real seismic data (a) with formation tops and (b) with the horizons. 74

Figure 5.3 The CDP gather for estimating effective coefficients. 75

Figure 5.4 Vertical interval velocities from sonic well log data. Blue line before block and red line after block. 76

Figure A-1 Geometry of a hyperbolic NMO equation and the shifted hyperbola NMO equation. (After Bancroft, private communication) 88

List of Symbols, Abbreviations and Nomenclature

Symbol	Definition
$A_0,\ A_2, A_4$	the coefficients of Taylor series
A_{4i}	quartic coefficient for layer i
AVO	amplitude versus offset
DMO	dip-moveout
$f_{i,j(i,l)}$	amplitude in trace i at the time sample j which varies with the zero-offset time sample l and the trace (offset) i
H	top layer thickness
HTI	horizontal transversely isotropic
r	lateral distance between the receiver and refraction point
RMS	root-mean-square
S	shift parameter
S_k	semblance coefficient for M traces
t	reflection traveltime between a source and a receiver
t_0	two-way zero-offset traveltime
$t_0^{(i-1)}(p)$	two-way traveltimes to the top and bottom of the layer i
$t_0(N)$	two-way vertical traveltime to the bottom of the layer N
$t_0(p)$	zero-offset time for the ray parameter p
TI	transversely isotropic
t_{h}	hyperbolic reflection traveltime between a source and a receiver
t_{P0}	zero-offset two-way reflection traveltime of P-wave
t_{p0}	two way vertical traveltimes for P-wave converted wave
t_{S0}	zero-offset two-way reflection traveltime of S-wave
t_{s0}	two way vertical traveltimes for P-SV converted wave
t_{sh}	The shifted hyperbolic reflection traveltime between a source and a receiver
Δt_{0i}	two-way vertical traveltime in layer i
$\Delta t_{0i}(p)$	two-way zero-offset traveltime through layer i for ray parameter p
NMO	normal-moveout
p	ray parameter
p	horizontal slowness
p_x	horizontal slowness in layer i
$p_{z,i}$	vertical slowness in layer i
q	vertical slowness
v_0	vertical velocity of compressional or shear waves
$v_0(\tau)$	interval vertical velocity
$v_{0,i}$	zero-offset phase velocity in layer i

v_{0i}	standing for α_0 for P-wave or β_0 for SV- or SH-waves in layer i
V_{h}	horizontal velocity for P-waves
v_{nmo}	interval NMO velocity for P-P or SV-SV waves
$v_{\mathrm{nmo},i}$	interval NMO velocity for P-P or SV-SV waves in layer i
$v_{\mathrm{nmo}}(\mathrm{P})$	normal moveout velocities of P-wave in single layer
$V_{\mathrm{NMO}}(\mathrm{P})$	normal moveout velocities of P-wave
$v_{\mathrm{nmo}}(p,t_{\mathrm{m}})$	interval NMO velocity as a function of vertical time t_{m}
$V_{\mathrm{NMO}}(\mathrm{SH})$	normal moveout velocities of SH-wave
$V_{\mathrm{NMO}}(\mathrm{SV})$	normal moveout velocities of SV-wave
$v_{\mathrm{ph},i}$	phase velocity in layer i
$v_{\mathrm{ph}}(\theta)$	phase velocity
$v_{\mathrm{P}}(\theta)$	phase velocity of P-wave
$V_{\mathrm{rms}}(N)$	vertical RMS velocity
VSP	vertical seismic profiles
$v_{\mathrm{SV}}(\theta)$	phase velocity of SV-wave
VTI	vertical transversely isotropic
V_{v}	average vertical velocity
$v(z)$	medium velocity
V_{γ}	skew moveout velocities
x	offset of a source and a receiver
$x_{\max}$	maximum offset of a gather
z	depth of reflectors of interest
z_i	thickness of layer i
α_0	vertical velocity of compressional waves
β_0	vertical velocity of shear waves
δ	$=4\left[v_{\mathrm{P}}(\pi/4)/\alpha_0-1\right]-\left[v_{\mathrm{P}}(\pi/2)/\alpha_0-1\right]$,an anisotropy parameter introduced by Thomsen
ε	$=\left(v_{\mathrm{P}}(\pi/2)-\alpha_0\right)/\alpha_0$, an anisotropy parameter introduced by Thomsen;
γ	$=\left(v_{\mathrm{SH}}(\pi/2)-\beta_0\right)/\beta_0$, an anisotropy parameter introduced by Thomsen
η	$=\left(\varepsilon-\delta\right)/\left(1+2\delta\right)$, a combination of Thomsen's anisotropy parameters
θ	phase angle
σ	$=(\alpha_0/\beta_0)^2(\varepsilon-\delta)$
$\tau-p$	Radon transform
τ_s	Time intercept of the asymptotes of the shifted hyperbola

$\Delta\tau_{0,i}$	two way interval zero-offset traveltime in layer i
$\Delta\tau_i$	two way traveltime in layer i
ζ_i	standing for anisotropy parameters δ_i, σ_i, or γ_i for the P-, SV-, or SH-wave in layer i

CHAPTER 1: INTRODUCTION

1.1. Motivation

One of the common assumptions in conventional seismic exploration is that the subsurface consists of a series of elastically homogeneous isotropic layers. In these layers, the moveout velocity derived from short-offset surface-seismic data is equivalent to the vertical root-mean-square (RMS) velocity (Taner and Koehler, 1969). Using these moveout velocities, we can convert reflection times to depth according to the Dix formulation (Dix, 1955) and carry out normal-moveout (NMO) or dip-moveout (DMO) correction, seismic data imaging and amplitude versus offset (AVO) analysis.

Numerous investigations during the previous decades have demonstrated the presence of seismic anisotropy in different geological settings and on various scales (Thomsen, 1986). These anisotropic effects may be produced by anisotropic layers, however, the effect may also result from a sequence of isotropic layers when the thickness of each layer is less than the wavelength of the elastic waves. Ignoring these anisotropy effects can adversely influence the results of most basic seismic data processing and interpretation steps, such as NMO correction, velocity analysis, stacking, migration, DMO correction, time-to-depth conversion, and AVO analysis (Banik, 1984; Thomsen, 1986; Winterstein, 1986; Larner, 1993; Alkhalifah and Larner, 1994; Tsvankin, 1995).

Thomsen in 1986 pointed out that there are three parameters controlling the properties of P, SV and SH-waves within the limits of weak anisotropy. These are so called Thomsen's anisotropy parameters ε, δ and γ. According to Thomsen (1986), these three "anisotropies" are appropriate combinations of elastic moduli which (1) simplify the relationships between phase velocity and elastic moduli; (2) are nondimensional; (3) reduce to zero in the case of isotropy. In vertical transverse isotropic media (anisotropic media with elastic properties that are the same in any direction perpendicular to a symmetry axis), the anisotropy parameters ε, δ and γ are defined by

$$\varepsilon = \frac{v_{\mathrm{P}}(\pi/2) - \alpha_0}{\alpha_0}, \tag{1.1}$$

$$\delta = 4\left[v_{\mathrm{P}}(\pi/4)/\alpha_0 - 1\right] - \left[v_{\mathrm{P}}(\pi/2)/\alpha_0 - 1\right], \tag{1.2}$$

$$\gamma = \frac{v_{\mathrm{SH}}(\pi/2) - \beta_0}{\beta_0}. \tag{1.3}$$

where α_0 and β_0 are vertical velocities of compressional and shear waves, respectively. The velocities $v_{\mathrm{P}}(\pi/2)$, $v_{\mathrm{SH}}(\pi/2)$ are the vertical velocity for P-wave and SH-waves, respectively. Figure 1.1 shows how ε and δ control the P wavefronts. In Figure 1.1(a), the values of ε are fixed at 0.2, and those of δ range from – 0.6 to 1.0 in increments of 0.2. In Figure 1.1(b), the values of δ are fixed at 0.2, and those of ε range from – 0.6 to 1.0 in increments of 0.2. Weak anisotropy assumes the magnitudes ε and δ are less than 0.2.

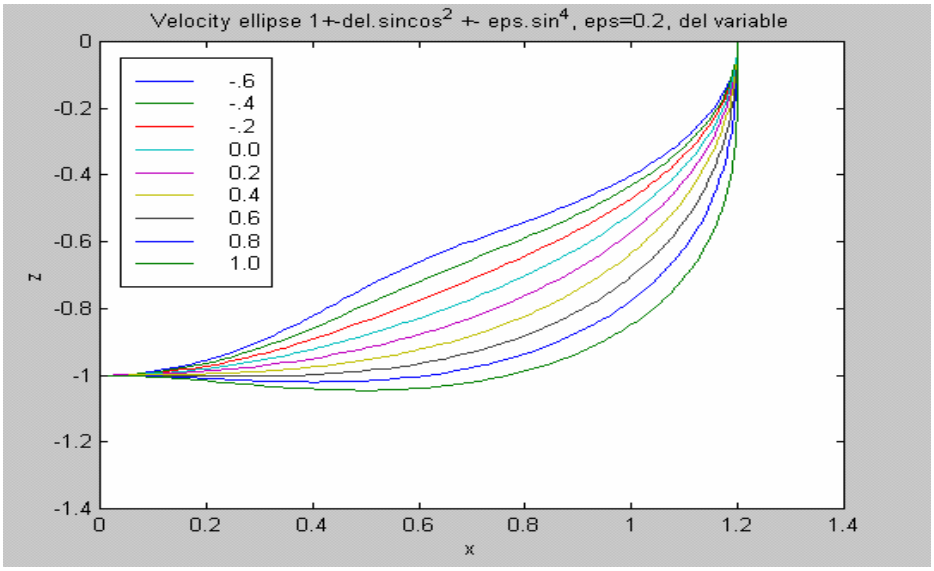

(a)

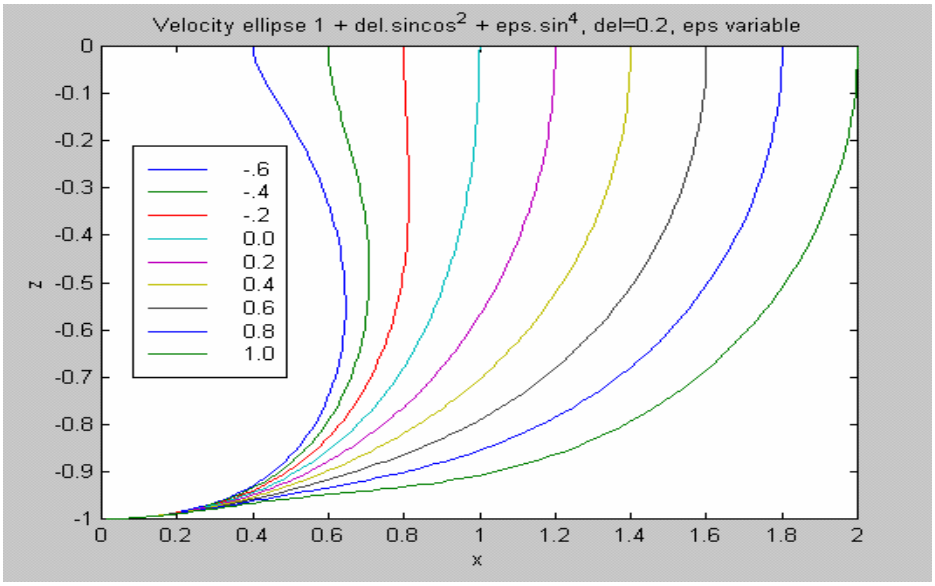

(b)

Figure 1.1 P wavefronts vary with anisotropy parameters ε and δ: (a) the values of ε are fixed at 0.2, and those of δ range from –0.6 to 1.0 in increments of 0.2. (b) the values of δ are fixed at 0.2, and those of ε range from –0.6 to 1.0 in increments of 0.2. (After John Bancroft, private communication)

Knowledge of the presence of anisotropy is important for accurate seismic imaging, time-to-depth conversion, and offers information on lithologic properties. The first and most important step in processing data in transversely isotropic (TI) media for which velocities vary with depth is parameter estimation. Several methodologies for performing anisotropy prestack imaging have appeared in the literature (Williamson et al., 1999). However, the key for successful anisotropic imaging is accurate estimation of the anisotropy parameters. One approach is to make educated assumptions based on prior geologic knowledge of the area from which appropriate values for the anisotropy parameters may be assumed. In other cases, which are the most common, the anisotropy parameters are estimated from the prestack seismic data (Alkhalifah, 1997a, Lou et al., Vestrum et al, 1999, Yan, L. et al, 2001) and well data (VSP, sonic logs) (Sexton and Williamson, 1998; Raymer et al., 1999). Consequently a systematic approach is desired to properly constrain the parameter estimation and obtain accurate subsurface images at the end of the depth imaging loop.

There are various methods to estimate anisotropy parameters. Wang (2002a) presented a method for measuring seismic velocities and transverse isotropy in rocks using a sing core plug. Wang pointed out that shale cores must be preserved. Otherwise, once a shale core is dehydrated, fractures will develop along the bedding plane, and the measured seismic velocities and anisotropy will no longer be accurate (Wang, 2002b).

Leslie et al (1998) determined the Thomsen anisotropic parameters ε and δ by measurement of headwave velocities along the seismic lines. This method obtained more realistic anisotropic parameters than those measured in the laboratory, but needs to ensure

that the spread is of sufficient length so that the refractor velocities measured are from rocks below the weathered layer.

Most methods for the estimation of Thomsen's anisotropy parameters are based on approximations of reflection coefficients (Ruger, 1998) and/or moveout velocities (Tsvankin, 1997). Traditionally, well log data are used in fracture detection. Such fracture detections are only valid at specific well locations. Since seismic data have wider spatial coverage than well data, quantitative fracture estimation from seismic data is of great practical importance. Anisotropy detection from conventional P-wave data has been limited to a few qualitative studies of the amplitude variation with offset (AVO) for different azimuthal directions (Allen, et al, 1993; Chang, et al, 1993; Mallick, et al, 1998; Ruger, et al, 1995). AVO studies rely on the reflection amplitudes rather than on reflection traveltimes.

Tsvankin et al (1995) examined the feasibility of inverting reflection traveltimes from horizontal interfaces for the parameters of a transversely isotropic model with a vertical symmetry axis. Various reflection traveltime methods are used to estimate anisotropy parameters in a VTI medium (White et al., 1983, Gaiser, 1990; Alkhalifah, et al 1995, Grechka and Tsvankin, 1998; Brown et al., 2000; Baan, et al, 2002, Elapavuluri and Bancroft, 2002; Isaac and Lawton, 2004). These methods form the main subject of this thesis. We compare different reflection traveltime methods of estimating anisotropy parameters so that for a particular dataset we can choose the best one.

1.2. Organization of the thesis

In Chapter 2, we begin with a literature review of various methods for estimating Thomsen's anisotropy parameters using seismic traveltime. Five types of methods for estimating seismic anisotropy parameters in VTI media are described and compared in this chapter. There is no perfect method for estimating anisotropy parameters. Each method has its own assumptions and limitations. The performance of each method depends on the particular data example under consideration and how well a particular dataset fits the assumptions of each method. The choice of anisotropy parameter estimation method should be based on knowledge of subsurface properties, geometry and wave mode of seismic data available, and objectives for estimating anisotropy parameters.

Chapters 3 to 4 are devoted to a comparison of various anisotropy moveout velocity analysis methods (including hyperbolic, shifted hyperbolic, modified three-term Taylor series and Alkhalifah's) used to estimate Thomsen's anisotropy parameters. In Chapter 3, we study the reflection-traveltime approximations of four moveout equations to true traveltime, and the approaches and formulations for estimating Thomsen's anisotropy parameters in layered anisotropic media.

We examine the estimation of Thomsen's anisotropy parameters in layered anisotropic media based on synthetic data in Chapter 4. In this chapter, we carry out four inversions on synthetic seismic data examples and try to determine the relationships

between the estimated anisotropy parameters and the true anisotropy parameters. Finally, we formulate some conclusions for guiding the application of these approximations.

We study the estimation of Thomsen's anisotropy parameters in layered anisotropic media based on field data in Chapter 5. In Chapter 4 we demonstrated the viability of the joint inversion of P-wave reflection traveltimes and well data to give Thomsen's anisotropy parameters, ε and δ, by applying it to synthetic data. However, the practical application of this approach to real data is a more challenging task. Firstly, application of the algorithm requires the recovery of nonhyperbolic moveouts from long-spread CMP gathers. Secondly, the semblance search at high incidence angles is also hindered by phase shifts in postcritical reflections. Thirdly, we have to consider the influence of noise on semblance. Chapter 5 describes the application of this inversion procedure to some real data from Blackfoot.

1.3. Contribution of the thesis

The accurate estimation of the velocity field is the most difficult step in imaging seismic data for anisotropic media. If anisotropy is applicable, then the methods described in this thesis provide a good starting model for improving larger volumes of data with, for example, reflection tomography. The main contributions in this thesis are as follows:

- Five reflection traveltime methods for estimating the anisotropy parameters ε and δ are compared and their advantages, limitations and assumptions are pointed out.

- Anisotropy moveout velocity analysis methods for the estimation of anisotropy parameters are investigated in detail. Four anisotropic moveout equations (including hyperbolic, shifted hyperbolic, modified three-term Taylor series and Alkhalifah's) are used to estimate anisotropy parameters in a VTI medium in combination with well-log data. Within its own offset range (hyperbolic, shifted hyperbolic, modified three-term Taylor series or Alkhalifah's), the accuracy of estimated δ decreases with offset and the accuracy of estimated ε increases with offset.

- Relationships between the inversion accuracy of four reflection-traveltime inversions in weakly anisotropic media and the spread length, subsurface anisotropy parameters, and offset ranges are quantitively described based on synthetic data. The results from the four reflection-traveltime inversions by semblance analysis for synthetic seismic examples demonstrate that in estimating δ, the Alkhalifah's and the shifted-hyperbolic estimations are better than the modified three-term Taylor-series method. Only the Alkhalifah's approximation can be used to estimate the anisotropy parameter ε accurately. Hyperbolic estimation is only suitable for estimation of elliptical anisotropy.

- The Alkhalifah's moveout velocity analysis technique is tested on both model data and real data. The tests show that if the objective is to obtain time-related seismic sections, moveout-velocity analysis at selected CMP locations along the line yields a robust velocity section. If, on the other hand, the objective is to derive interval coefficients from Dix-type differentiation in order to obtain

depth-related seismic sections, then the time interval should be larger than 200 ms to yield results that are geologically plausible.

CHAPTER 2: DIFFERENT METHODS FOR ESTIMATING THOMSEN'S ANISOTROPY PARAMETERS(LITERATURE REVIEW)

It is usually true that, in looking into the future, people can benefit by reviewing the accomplishments of the past. In this Chapter, we review five categories of methods (phase slowness methods, direct traveltime inversion methods, $\tau - p$ methods, DMO inversion methods, and anisotropy moveout velocity analysis methods) for estimating anisotropy parameters in VTI media and present their corresponding inversion steps. Then, we compare various aspects of these methods such as suitable media, spread length, and wave modes, data types and geometry, and accuracy. Finally, we reach some conclusions for guiding their application.

2.1. Phase slowness methods

In practice, transverse isotropy may be suitably approximated by elliptical anisotropy at small angles of incidence (Vander Stoep, 1966). For elliptically anisotropic media in VSP geometry, estimating anisotropy parameters in the $\tau - p$ domain is routinely applied in multi-offset vertical seismic profiles (VSPs). Local estimates of horizontal and vertical slownesses can be obtained for each source-receiver combination by computing the differential moveout between sources for a fixed receiver and vice versa. In a laterally homogeneous earth model, these estimates can then be combined to yield the complete phase slowness surface at each depth, thereby allowing for an estimation of the anisotropy parameters with depth (White et al, 1983; Gaiser, 1990;

Schmitt and Kebaili, 1993; Miller et al., 1994). We refer to these as phase slowness methods since the phase velocities are found from horizontal and vertical phase slowness.

White et al. (1983) and Gaiser (1990) developed the phase slowness methods. Their methods are similar in that vertical and horizontal slownesses are discovered and used to calculate phase-velocity magnitudes and directions under the assumption that planar wavefronts pass the receivers. Their methods differ in that Gaiser's method extracts transversely isotropic phase velocities from a vertical seismic profile consisting of multi-offset surface sources and multi-receiver depths in a single wellbore (Figure 2.1 and 2.2), whereas White et al.'s method extracts transversely isotropic phase velocities from vertical seismic profiles of two closely spaced boreholes (Figure 2.3). These phase-slowness methods are based on estimates of, for the VTI case, the horizontal slowness, p, and the vertical slowness, q. By assuming that the medium is laterally homogeneous and elliptically anisotropic, the amplitude and the direction of the phase velocity $v_{\text{ph}}(\theta)$ can be calculated by the equations

$$v_{\text{ph}} = \left(p^2 + q^2\right)^{-\frac{1}{2}} \tag{2.1}$$

$$\theta = \tan^{-1}\left[p/q\right], \tag{2.2}$$

where p and q can be obtained by $p = \frac{dt}{dx} \approx \frac{\Delta t}{\Delta x}$ and $q = \frac{dt}{dz} \approx \frac{\Delta t}{\Delta z}$, respectively. We can estimate the anisotropy parameters by best fitting the data with the theoretical phase velocity formulae.

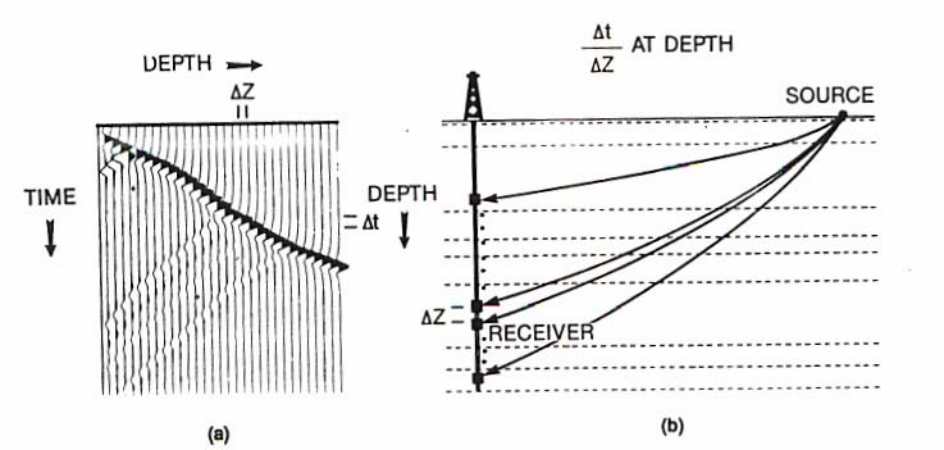

Figure 2.1 Vertical slowness at depth. (a) Synthetic P-wave offset VSP illustrating vertical slowness estimate $\Delta t / \Delta z$. (b) The model consists of receiver depths ranging from 213.36 to 670.56 m at 15.24 m intervals and source offsets of 457.2 m. (After Gaiser, 1990)

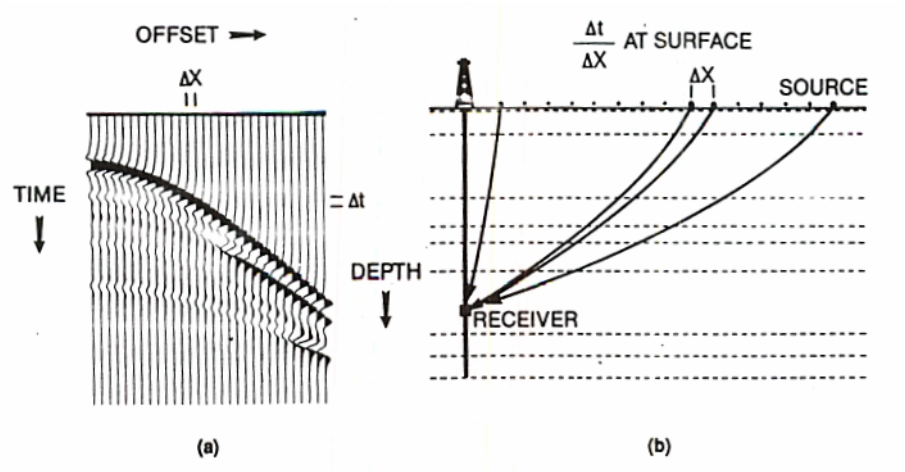

Figure 2.2 Horizontal slowness at surface. (a) Synthetic P-wave offset VSP illustrating horizontal slowness estimate $\Delta t / \Delta x$. (b) The model consists of receiver depths from 487.68 m and source offsets ranging from 30.48 to 914.4 m at 30.48 m intervals. (After Gaiser, 1990)

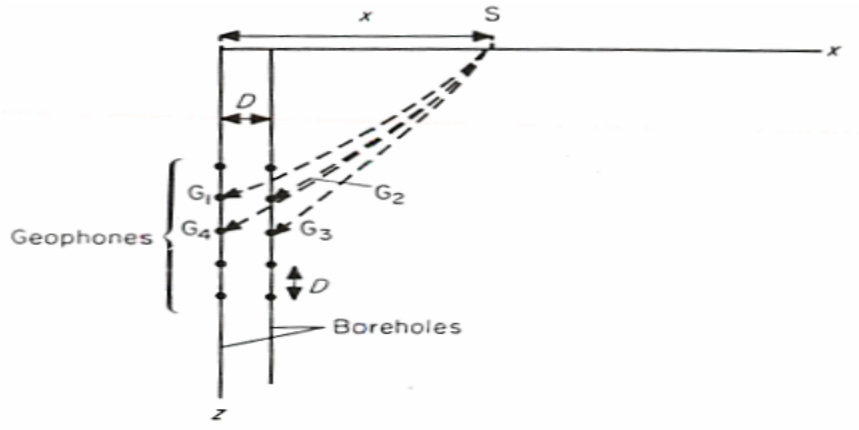

Figure 2.3 Description of the field experiment for a given location of the source. (After White et al., 1983)

2.2. Direct traveltime inversion methods

For elliptically anisotropic media in VSP geometry, Brown et al. (2000) presented a direct traveltime inversion of VSP data for anisotropy parameter estimation.

This method directly uses measured traveltimes in estimating anisotropy parameters under the assumption that (1) the media is elliptically anisotropic; (2) the depth of the interface is known, and (3) the velocity field of the overburden is assumed to be known.

Using the symbols shown in Figure 2.4, the traveltime t between a point source and a point receiver is:

$$t = t_1(r) + \frac{\sqrt{\frac{r^2}{1+2\xi} + Z^2}}{v_0} \quad , \tag{2.3}$$

where $\xi = \gamma$ for SH-wave or $\xi = \delta$ for P-wave in the layer of interest; $t_1(r)$ is the traveltime for the upper medium; $v_0 = \alpha_0$ for P-wave, $v_0 = \beta_0$ for SH-wave, obtained from zero offset VSP data; Z is the depth of the receiver in the buried layer and r corresponds to the lateral distance between the receiver and the refraction point in Figure 2.4. Equation (2.3) can be rewritten into:

$$\xi = \frac{1}{2}\left\{\frac{r^2}{v_0^2\left[t - t_1(r)\right]^2 - Z^2} - 1\right\}. \tag{2.4}$$

According to Fermat's principle of stationary time, the property of Equation (2.3) that t decreases with increasing ξ, and certain mathematic arrangement, Brown et al. (2000)

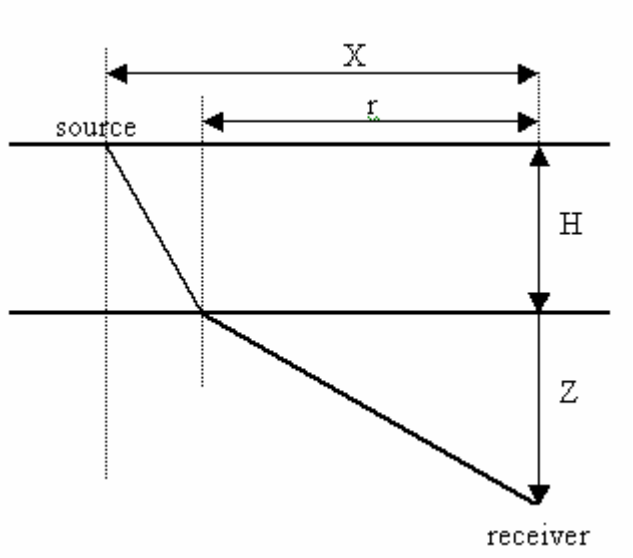

Figure 2.4 The two-layer model. *H* denotes top layer thickness. *Z* gives the depth of the receiver in the buried layer. The horizontal source-receiver offset is denoted as *X*. The symbol *r* corresponds to the lateral distance between the receiver and the refraction point. (After Brown et al., 2000)

proved that $\frac{\partial \xi}{\partial r} = 0$ and $\frac{\partial^2 \xi}{\partial r^2} > 0$ for a minimum time $t(r, \xi)$. This indicates that the anisotropy parameter ξ is also a minimum, so we can get the value of r from $\frac{\partial \xi}{\partial r} = 0$ and then get anisotropy parameter ξ directly from Equation (2.4).

2.3. $\tau - p$ methods

At the limits of weak anisotropy, group velocities may be approximated with the expressions for the phase velocities (Thomsen, 1986). However, for an arbitrary strength of anisotropy, the mathematical expression relating group to phase velocities is rather awkward (Musgrave, 1970; Thomsen, 1986). To solve this problem, plane-wave decompositions such as the slant stack (also known as the $\tau - p$ or Radon transform) can be applied to the seismic data (Hake, 1986; Baan and Kendall, 2002). In this case, the data are transformed to the intercept time versus the slowness domain, and phase velocities are directly extracted as a function of the horizontal slowness. We can calculate exact traveltimes of reflected P- and SV-waves and estimate anisotropy parameters. Since this method estimates anisotropy parameters in the $\tau - p$ domain, we refer to it as the $\tau - p$ method.

In addition, Tsvankin and Thomsen (1994) show that while the P-wave moveout is usually relatively smooth up to at least $x = 2z$ where the SV-wave traveltime curves can exhibit a sharp change in moveout velocity. Figure 2.5 is a plot of the squared traveltime t versus the squared normalized offset (x/z) where z is the depth of the reflector. For a hyperbolic curve, this plot should be linear, but is distorted when SV-wave traveltime

curves exhibit a sharp change in moveout velocity at $x = (1.7 \rightarrow 2.0)z$ .This is caused by the influence of the velocity maximum located at incidence angles near 45 degrees (i.e., up to the first kink or cusp on the wave surface). Figure 2.5 illustrates the velocities that vary with offset that include a cusp. Here $\sigma = \left(\alpha_0^2 / \beta_0^2\right)(\varepsilon - \delta) = 1.276 > 0,$ σ represents the deviation from ellipticity (Vestrum et al, 1999). $\alpha_0 = 3.048$ km/s, $\beta_0 = 1.490$ km/s, $\varepsilon = 0.255$, $\delta = -0.05$. Consequently it is very difficult to recover the analytical value of the SV-wave short-spread moveout velocity. To solve these problems, Baan and Kendall (2002) presented a new method to calculate exact traveltimes of reflected P- and SV-waves and to estimate anisotropy parameters in the $\tau - p$ domain.

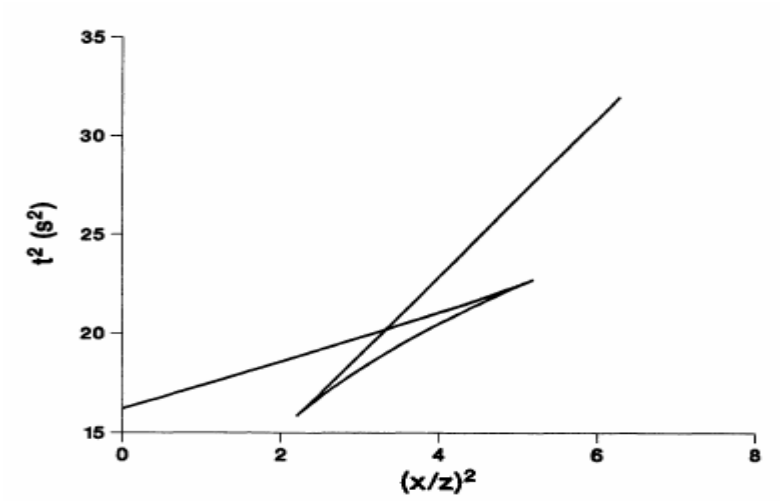

Figure 2.5 SV-wave moveout curve with a cusp. Model parameters are (from Thomsen, 1986): $\alpha_0 = 3.048$ km/s, $\beta_0 = 1.490$ km/s, $\varepsilon = 0.255$, $\delta = -0.05$ ($\sigma = 1.276$), $z = 3$ km. (After Tsvankin and Thomsen, 1994)

Moveout curves in the $\tau - p$ domain

The moveout curves in the $\tau - p$ domain are described as follows (Baan and Kendall, 2002):

$$\tau = 2\sum_i z_i p_{z,i} = \sum_i \Delta\tau_i \tag{2.5}$$

$$\Delta\tau_i^2 / \Delta\tau_{0,i}^2 = \frac{\left(2z_i p_{z,i}\right)^2}{\left(2z_i / v_{0,i}\right)^2} = \frac{v_{0,i}^2}{v_{\mathrm{ph},i}^2}\left[1 - p_x^2 v_{\mathrm{ph},i}^2\right], \tag{2.6}$$

where $\Delta\tau_{0,i}$ is the two-way interval zero-offset traveltime in layer i, and $v_{0,i}$ is its associated phase velocity; $v_{\mathrm{ph},i}$ is the phase velocity in layer i; p_x and $p_{z,i}$ are horizontal and vertical slownesses in layer i (note that p_x remains constant for a given ray for all layers); z_i is the thickness of layer i, and $\Delta\tau_i$ is the two-way traveltime in layer i.

For homogeneous isotropic media, the hyperbolic reflection moveouts in the *x*-*t* domain (CMP gather) are transformed to ellipses in the τ -*p* domain since the phase velocity remains constant everywhere independent of horizontal slowness. For anisotropic media, Equation (2.6) accurately describes the nonelliptical curves for anisotropic models displaying a horizontal symmetry plane if the phase velocity as a function of the horizontal slowness is known.

For P-wave, we know the expression of phase velocity $v_{\mathrm{P}}(\theta)$ in terms of phase angle θ (Tsvankin, 1996) as:

$$v_{\mathrm{P}}^2(\theta)=\alpha_0^2\left[1+\varepsilon\sin^2\theta-\frac{f}{2}+\frac{f}{2}\sqrt{1+\frac{4\sin^2\theta}{f}(2\delta\cos^2\theta-\varepsilon\cos 2\theta)+\frac{4\varepsilon^2\sin^4\theta}{f^2}}\right], \qquad (2.7)$$

where $f=1-\beta_0^2/\alpha_0^2$.

Using Snell's law, $\sin\theta=v_{\mathrm{P}}p_x$, we can obtain the expression of phase velocity $v_{\mathrm{P}}(p_x)$ in terms of horizontal slowness p_x (Baan and Kendall, 2002) as:

$$v_{\mathrm{P}}^2(p_x)=\frac{\alpha_0^2(2-f+2(\delta f-\varepsilon)p_x^2\alpha_0^2+f\sqrt{s_P})}{2-4\varepsilon p_x^2\alpha_0^2-4f(\varepsilon-\delta)p_x^4\alpha_0^4} \qquad (2.8)$$

where $s_{\mathrm{P}}=1+4\left(\frac{2\delta-\varepsilon}{f}-\delta\right)p_x^2\alpha_0^2+8\left(\delta^2/2+\delta-\varepsilon+\frac{\varepsilon-\delta-\delta\varepsilon}{f}+\frac{\varepsilon^2}{2f^2}\right)p_x^4\alpha_0^4$.

Now that the phase velocity as a function of the horizontal slowness is known, exact moveout curves can be calculated for arbitrary anisotropy without the need for any Taylor-series approximation or raytracing.

Equation (2.6) also describes the form of the $\tau(p_x)$ curves of direct waves recorded in a VSP geometry, with the difference that the curves should be normalized with the one-way interval zero-offset times.

Using an acoustic approximation (i.e., $\beta_0=0$, $f=1$), we can get a two-parameter ($V_{\mathrm{NMO}}(\mathrm{P})$ and η) expression for P-wave from Equations (2.6) and (2.8). That is,

$$\tau^2(p_x)/\tau_0^2=\alpha_0^2p_z^2=1-\frac{p_x^2v_{\mathrm{nmo}}^2(\mathrm{P})}{1-2\eta p_x^2v_{\mathrm{nmo}}^2(\mathrm{P})}, \qquad (2.9)$$

where

$$\eta = \frac{\varepsilon - \delta}{1 + 2\delta}. \tag{2.10}$$

Figure 2.6 shows layer stripping in the $\tau - p$ domain.

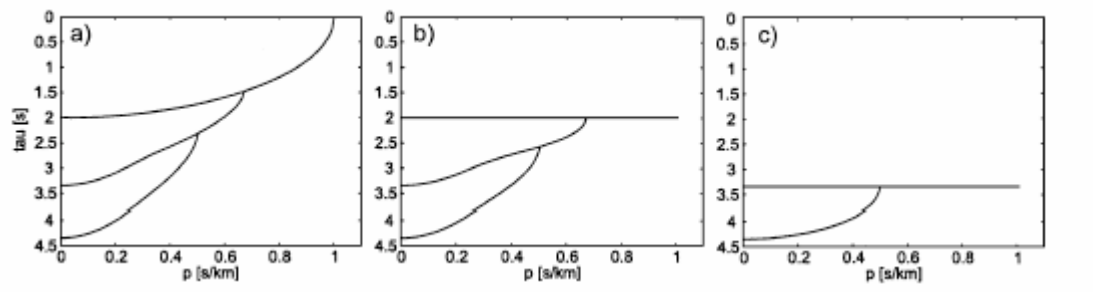

Figure 2.6 Layer stripping in the $\tau - p$ domain: (a) $\tau - p_x$ curves; (b) first layer removed; (c) top two layers removed. (After Baan and Kendall, 2002).

Using Equations (2.6), (2.8) and (2.9), we can estimate anisotropy parameters for P-waves. The procedure is as follows:

1) Transform the seismic data into the $\tau - p$ domain using the equation $t = \tau + p_x x$;
2) Pick the semielliptical $\tau(p_x)$ curves for several reflectors (see Figure 2.6(a));
3) Calculate the differential intercept times $\Delta\tau = \tau_i - \tau_{i-1}$;

4) The observed $\Delta\tau_i(p_x)$ curves are fitted, using Equation (2.8) for the P-waves, layer by layer, from the shallowest to the deepest layer, to obtain the anisotropy parameters $v_{nmo}(P)$ and η of each interval separately.

2.4. DMO inversion methods

It has been proven that sometimes it is not necessary to know the individual values of the anisotropy parameters and the vertical velocity for P-wave time processing (Alkhalifah and Tsvankin, 1995). All time-processing steps, including NMO, DMO, and time migration, are fully determined by the two parameters V_{NMO} and η which are responsible for reflection moveout. The parameter η is defined by

$$\eta = 0.5\left(\frac{V_{\mathrm{h}}^2}{V_{\mathrm{NMO}}^2} - 1\right) = \frac{\varepsilon - \delta}{1 + 2\delta}. \tag{2.11}$$

There are two ways to estimate V_{NMO} and η. Alkhalifah and Tsvankin (1995) developed an inversion procedure designed to obtain V_{NMO} and η from NMO velocities measured for two different reflectors dips. Usually, V_{NMO} can be obtained directly by conventional semblance analysis of horizontal events, whereas η is obtained from the NMO velocity of an additional dipping event. This is sometimes known as the DMO inversion method.

The NMO velocity for dipping events in a homogeneous anisotropic medium depends on v_{nmo} and η (when $\beta_0 = 0$) as follows (Alkhalifah, 1998):

$$v_{\mathrm{nmo}}^2(p) = v_{\mathrm{nmo}}^2(0)\frac{1+4\eta y^2-6\eta(1+2\eta)y^4}{\left(1-2\eta y^2\right)\left(1-(1+2\eta)y^2\right)\left(1-4\eta y^2+2\eta(1+2\eta)y^4\right)}, \tag{2.12}$$

where $y = v_{\mathrm{nmo}}(0)p$, and p is ray parameter.

For horizontal layers, whether the medium is isotropic or VTI, the NMO velocity $V_{\mathrm{NMO}}(t_0)$ at a certain zero-offset time t_0, is given by an rms relation (Hake et al., 1984; Tsvankin and Thomsen, 1994) as follows:

$$V_{\mathrm{NMO}}^2(t_0) = \frac{1}{t_0}\int_0^{t_0} v_{\mathrm{nmo}}^2(\tau)d\tau \ , \tag{2.13}$$

where $v_{\mathrm{nmo}}(\tau)$ are interval NMO velocities given by

$$v_{\mathrm{nmo}}(\tau) = v_0(\tau)\sqrt{1+2\delta(\tau)} \ \ ; \tag{2.14}$$

and $v_0(\tau)$ is the interval vertical velocity. For dipping reflectors beneath a horizontally layered medium, when expressed in terms of ray parameter p, NMO velocity along the zero-offset raypath is also given by a similar rms relation (Alkhalifah and Tsvankin, 1995):

$$V_{\mathrm{NMO}}^2(p,t_0(p)) = \frac{1}{t_0(p)}\int_0^{t_0(p)} v_{\mathrm{nmo}}^2(p,t_{\mathrm{m}}(\tau))d\tau, \tag{2.15}$$

where $v_{\mathrm{nmo}}(p,t_{\mathrm{m}})$ is the interval NMO velocity as a function of vertical time (migrated time) t_{m} and ray parameter p, and $t_0(p)$ is the zero-offset time for the ray parameter p. This ray parameter is the half slope, in the zero-offset domain, of the reflection from the

dipping reflector at time $t_0(p)$ used to measure $v_{\text{nmo}}(p,t_{\text{m}})$, and $t_0(0)=t_{\text{m}}$ is the two-way traveltime to a horizontal reflector.

The integral in Equation (2.15) can be expressed in terms of migrated time, t_{m}, as follows:

$$V^2_{\text{NMO}}(p,t_0(p))=\frac{1}{t_0(p)}\int_0^{t_{\text{m}}} v^2_{\text{nmo}}(p,\tau)\frac{\mathrm{d}t_0(p)}{\mathrm{d}\tau}\mathrm{d}\tau\,. \tag{2.16}$$

For horizontal reflectors ($p=0$), $\mathrm{d}t_0(p)/\mathrm{d}\tau=1$. For dipping reflectors, $v_{\text{nmo}}(p,\tau)$ depends only on the interval values $v_{\text{nmo}}(0,\tau)$ and $\eta(\tau)$ in each layer or, equivalently, at each time sample (see Equation (2.12)). Alkhalifah and Tsvankin (1995) show that $t_0(p)$ is a function of the medium parameters $v_{\text{nmo}}(0)$ and η, as well as the vertical time, with the form

$$t_0(p)=t_{\text{m}}f[\eta,v_{\text{nmo}}(0),p]\,. \tag{2.17}$$

Thus,

$$\frac{\mathrm{d}t_0(p)}{\mathrm{d}t_{\text{m}}}=f[\eta,v_{\text{nmo}}(0),p], \tag{2.18}$$

where f is the operator that relates the vertical time to the zero-offset time.

For isotropic media, $\eta=0$, and

$$f[v_{\text{nmo}}(0), p] = \frac{1}{\sqrt{1 - p^2 v_{\text{nmo}}^2(0)}} \ . \tag{2.19}$$

For TI media, f can be obtained through raytracing.

Equation (2.15), when expressed in terms of homogeneous layers, is given by

$$\left(V_{\text{NMO}}^{(N)}(p)\right)^2 = \frac{1}{t_0(p)} \sum_{i=1}^{N} \left(v_{\text{nmo},i}(p)\right)^2 \Delta t_{0i} \ , \tag{2.20}$$

where $\Delta t_{0i}(p)$ is the two-way zero-offset traveltime through layer i for ray parameter p. The interval NMO velocity in any layer i can be obtained by applying the Dix formula (Dix, 1955) to the NMO velocities at the top $V_{\text{NMO}}^{(i-1)}$ and bottom $V_{\text{NMO}}^{(i)}$ of the layer i:

$$\left(v_{\text{nmo},i}(p)\right)^2 = \frac{t_0^{(i)}(p)\left(V_{\text{NMO}}^{(i)}(p)\right)^2 - t_0^{(i-1)}(p)\left(V_{\text{NMO}}^{(i-1)}(p)\right)^2}{t_0^{(i)}(p) - t_0^{(i-1)}(p)}, \tag{2.21}$$

where $t_0^{(i-1)}(p)$ and $t_0^{(i)}(p)$ are the two-way traveltimes to the top and bottom of the layer i, respectively, calculated along the ray given by the ray parameter p for normal-incidence reflection from the dipping reflector that is used in measuring stacking velocity. All NMO velocities here correspond to a single ray-parameter value p. Clearly, the recovery of $v_{\text{nmo},i}(p)$ requires obtaining the moveout velocities in the overlying medium for the same value of the ray parameter.

2.5. Anisotropy moveout velocity analysis methods

According to Thomsen's paper (1986), there is a relationship between normal moveout velocities and anisotropy parameters in a homogeneous anisotropic layer as follows:

$$V_{\mathrm{NMO}}(\mathrm{P}) = \alpha_0\sqrt{1+2\delta}\ , \tag{2.22a}$$

$$V_{\mathrm{NMO}}(\mathrm{SV}) = \beta_0\sqrt{1+2\frac{\alpha_0^2}{\beta_0^2}(\varepsilon-\delta)}\ , \tag{2.22b}$$

$$V_{\mathrm{NMO}}(\mathrm{SH}) = \beta_0\sqrt{1+2\gamma}\ , \tag{2.22c}$$

where $V_{\mathrm{NMO}}(\mathrm{P})$, $V_{\mathrm{NMO}}(\mathrm{SV})$ and $V_{\mathrm{NMO}}(\mathrm{SH})$ are normal moveout velocities of P-, SV-, and SH-wave, respectively, and can be obtained from short-spread surface seismic data; ε, δ and $\sigma = (\alpha_0/\beta_0)^2(\varepsilon-\delta)$ are anisotropy parameters introduced by Thomsen (1986); α_0 and β_0 are vertical velocities of compressional and shear waves, respectively.

Although the parameters ε, δ and σ were originally introduced to simplify velocity equations for weakly anisotropic media, Tsvankin and Thomsen (1994) pointed out that they also facilitate moveout analysis for transversely isotropic models with arbitrary strengths of anisotropy.

It is clear from Equations (2.22a-c) that NMO velocities do not provide enough information to recover all the anisotropy parameters, even if both P and shear data have

been recorded. This is because there are five unknown parameters ($\alpha_{0,}$ $\beta_{0,}$ ε, δ, and γ) and only three equations.

For arbitrary strengths of anisotropy, when one of two vertical velocities ($\alpha_{0,}$ or β_0) is known (by check shot or well log), we can estimate anisotropy parameters using Equations (2.22a-c) in combination with the equation $\alpha_0 / \beta_0 = t_{S0} / t_{P0}$ by solving the four equations with four unknown parameters ($\alpha_{0,}$ or $\beta_{0,}$ ε, δ, and γ). This is so called hyperbolic moveout velocity analysis methods in this paper.

For elliptical anisotropy, we have:

$$V_{\mathrm{NMO}}(\mathrm{P}) = \alpha_0 \sqrt{1+2\delta} \tag{2.23a}$$

$$V_{\mathrm{NMO}}(\mathrm{SV}) = \beta_0 \tag{2.23b}$$

$$V_{\mathrm{NMO}}(\mathrm{SH}) = \beta_0 \sqrt{1+2\gamma} \ . \tag{2.23c}$$

We can estimate anisotropy parameters using Equations (2.23a-c) in combination with the equation $\alpha_0 / \beta_0 = t_{S0} / t_{P0}$ by solving the four equations for four unknown parameters ($\alpha_{0,}$ $\beta_{0,}$ δ, and γ). For elliptically anisotropic media, the moveout velocity is equal to the horizontal velocity (Banik, 1984; Tsvankin and Thomsen, 1994).

There are various approaches for estimating anisotropy parameters using anisotropy moveout velocity analysis (Alkhalifah and Tsvankin, 1995; Grechka and Tsvankin, 1998; Elapavuluri and Bancroft, 2002). Elapavuluri and Bancroft (2002) showed the shifted

hyperbolic approximation can also be used to estimate anisotropy parameters from P-wave reflection data.

Besides hyperbolic approximation and the shifted hyperbolic approximation, a popular approach for estimating anisotropy is a modified three-term Taylor series approximation to the reflection moveout curve (Tsvankin and Thomsen, 1994; Alkhalifah and Larner, 1994; Tsvankin, 1995).

If one ignores the contribution of the vertical shear-wave velocity, a modified three-term Taylor-series approximation to the reflection moveout curve can be fully determined by two parameters, either V_{NMO} (NMO velocity) and $\eta = (\varepsilon - \delta)/(1 + 2\delta)$ (Alkhalifah and Tsvankin, 1995); or V_{NMO} and V_{h} (horizontal velocity). Based on the Alkhalifah's moveout, a 2-D semblance scan can be used to estimate anisotropy parameters. For convenience, we refer to this method as Alkhalifah's reflection-traveltime inversion.

The hyperbolic moveout velocity analysis, shifted hyperbolic, modified three-term Taylor series and Alkhalifah's inversion methods have similar procedures for estimation of Thomsen's anisotropy parameters. They are our focus in this thesis. We will discuss them later in this Chapter and in Chapters 3 and 4.

2.6. An initial comparison of different methods

We have presented five types of methods for estimating anisotropy parameters using reflection traveltime. They are: (1) phase slowness methods; (2) direct traveltime inversion methods; (3) $\tau - p$ methods; (4) DMO inversion methods and (5) anisotropy

moveout velocity analysis methods. The latter category includes hyperbolic moveout velocity analysis, shifted hyperbolic moveout velocity analysis, modified three-term Taylor-series moveout velocity analysis as well as Alkhalifah's moveout velocity analysis. Each method has its own assumptions and limitations. It is necessary to compare them for guiding their application.

2.6.1 *A comparison of hyperbolic moveout velocity analysis, phase slowness and direct traveltime inversion methods*

As mentioned above, hyperbolic moveout velocity analysis methods are performed on short offset data on the basis of hyperbolic approximation of traveltimes and require a prior knowledge of one of two vertical velocities (by shot check or well log). Therefore, these methods have the disadvantage that they rely on sonic-log velocities which, due to frequency dispersion effects, typically differ from seismic velocities by approximately 5 %. This error could adversely affect the estimation of the true anisotropy which, in many cases, is of the same scale (Vander Stoep, 1966). These methods, however, can be used in absence of pure shear-wave data. There are two benefits to this: (1) According to Tsvankin and Thomsen's paper (1994), the SV-wave moveout at small offsets can become strongly nonhyperbolic if σ is negative ($\varepsilon < \delta$) whereas the P-SV wave does not exhibit the same anomalous nonhyperbolic moveout at very small offsets for $\sigma < 0$. Therefore, the short offset P and P-SV moveouts can usually recover the analytical value of the SV-wave short-offset moveout velocity. (2) Direct recording of shear waves can be avoided because direct recording of shear waves is expensive and logistically difficult, particularly in a marine environment.

Phase slowness methods find phase velocities by determining slowness on the basis of traveltime differences between adjacent detectors. This means that the adjacent receivers or sources should be spaced closely enough such that there is negligible curvature of the wavefront between the detectors. The methods also require the same elevation of sources at the same elevation, and receivers at the same horizontal location. In addition, the experiment for phase slowness methods, which consists of many depths and surface source offsets, is in practice difficult and expensive to perform.

Unlike the phase slowness methods, direct traveltime inversion methods do not depend on surface topography and the shape of the wellbore. In a numerical example presented by Brown et al (2000), typical VSP yield errors from the phase slowness methods were about 25 times greater than those by the direct traveltime methods. Furthermore, in cases where the VSP has been acquired with a single source offset, the direct traveltime methods will at least produce some results, whereas the phase slowness methods will not.

Both phase slowness methods and direct traveltime methods assume no lateral velocity variation and elliptical anisotropy. In addition, direct traveltime inversion methods also assume that 1) the depth of the interface is known, and (2) the velocity field of the overburden is assumed to be known. This means that phase slowness methods are more general than direct traveltime inversion methods.

Table 2.1 A comparison of hyperbolic moveout velocity analysis, phase slowness and direct traveltime inversion methods

	Hyperbolic	Phase Slowness	Direct Traveltime
VTI media	Elliptical	Elliptical	Elliptical
Spread	*X*<*Z*	*X*<*Z*	*X*<*Z*
Data	Surface	VSP	VSP
Wave mode	P, SV or P-SV,SH	P,SV,SH	P or SH
Inversion	Dix-type differentiation	Fitting	Analytical
Advantages	Converted wave	No prior knowledge of subsurface	Accuracy, less requirement for topography
Limitation	Vertical velocity	Acquisition	Limited case

Table 2.1 summarizes the comparison between hyperbolic moveout velocity analysis, phase slowness and direct traveltime inversion methods.

2.6.2 A comparison of the modified three-term Taylor series, shifted hyperbolic and $\tau - p$ methods

Modified three-term Taylor series approximation methods and shifted hyperbolic methods are performed on intermediate-spread ($z < x_{\max} < 2z$) or long-spread ($x_{\max} > 2z$) data for P-wave on the basis of nonhyperbolic approximations of traveltimes and assumptions for weak anisotropy, small angle, or arbitrary strength of anisotropy approximations. Therefore, these methods have the disadvantage that they rely on the quality of long offset seismic data, which could affect the estimation of the true anisotropy. As with hyperbolic moveout methods, however, these methods can be used in absence of pure shear-wave data.

The $\tau - p$ methods estimate anisotropy parameters using the $\tau - p$ transform and have the advantage to estimating anisotropy parameters without the need for any raytracing. Another advantage is that the phase velocity is the natural velocity to work with in anisotropic media and that exact expressions for phase velocity exist for VTI, HTI, and even orthorhombic media (Tsvankin, 1997). Like the modified three-term Taylor-series methods and shifted hyperbolic methods, however, the offset for $\tau - p$ methods needs to be at least 2–2.5 times the depth of the reflector of interest (Alkhalifah, 1997a). This is a limitation for the modified three-term Taylor-series, shifted hyperbolic, and $\tau - p$ methods. Therefore, high-quality data are needed to pick traveltimes or $\tau(p_x)$ curves to such offsets. In addition, the principal relation describing the form of the $\tau - p$ curves, Equation (2.6), is only valid for pure-mode phases and anisotropic systems displaying a horizontal symmetry plane (like VTI, HTI, and orthorhombic media with a symmetry axis parallel to the z-axis).

The $\tau - p$ method has a greater accuracy than the Taylor-series expansion (Tsvankin and Thomsen, 1994). Moreover, it can handle both cusps and kinks in the SV-wave moveout curves that cannot be handled by the modified three-term Taylor series methods and shifted hyperbolic methods (Figure 2.7). Furthermore, a layer-stripping procedure can be more easily applied in the $\tau - p$ domain than in the $t - x$ domain such that both effective (average) and local (interval) estimates can be obtained.

Due to the reduction of the number of parameters involved, the vertical P-wave velocity cannot be assessed using P-wave moveout only, and no time-to-depth conversion

is possible without well log information. On the other hand, this drawback does not exist for pure-mode SV-data. The vertical SV-wave velocity is provided by the inversion method. This may be a further reason to advocate the acquisition of pure-mode shear-wave data for exploration purposes. However, SV waves can suffer from poor signal-to-noise ratios and phase reversals, the effects of which on parameter estimation will need to be addressed (Baan and Kendall, 2002).

Table 2.2 summarizes the comparison of the modified three-term Taylor series, shifted hyperbolic and $\tau - p$ methods.

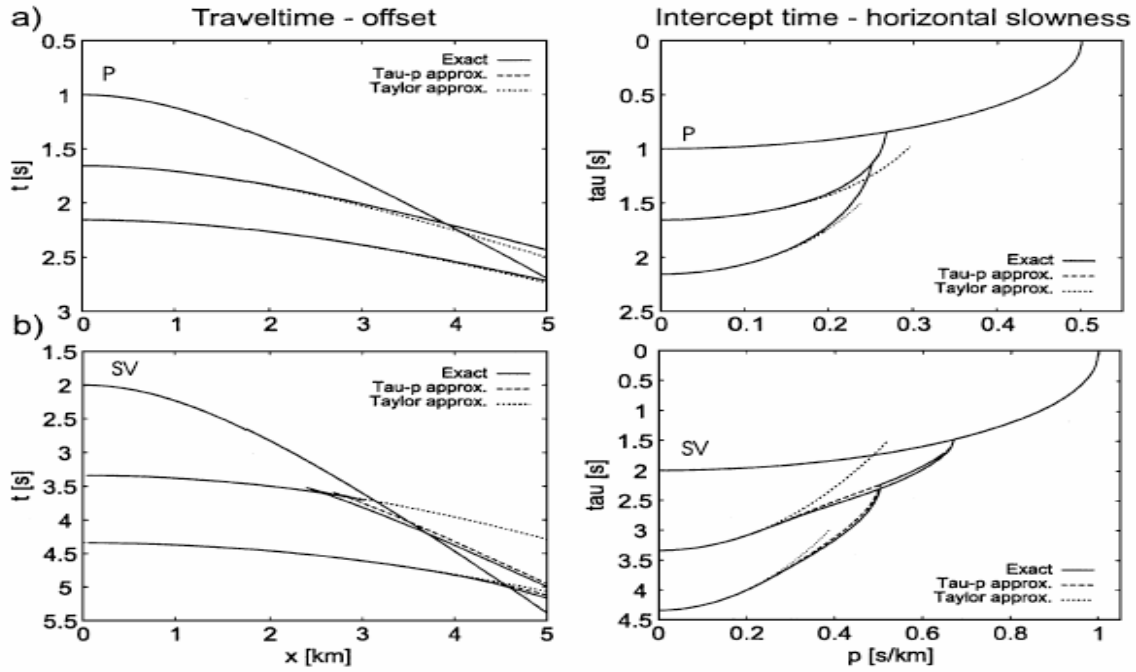

Figure 2.7 Moveout and $\tau(p_x)$ curves of the three-layer model for (a) P-wave and (b) SV-wave. Only the second layer is anisotropic. Solid line: exact curves; long dashes: $\tau - p$ method using reduced-parameter expression; short dashes: Taylor series approximation (After Baan and Kendall, 2002).

Table 2.2 A comparison of the modified three-term Taylor series, shifted hyperbolic and $\tau - p$ methods

	Modified three-term Taylor	Shifted hyperbolic	$\tau - p$ method
VTI media	Weak	Weak	Arbitrary
Spread	$z<x<2z$ $z<x<1.0\,z$ for P-wave	$z<x<2z$ $z<x<1.5z$ for P-wave	$z<x<2z$ $z<x<1.5z$ for P-wave
Data	Surface, VSP	Surface , VSP	Surface , VSP
Wave mode	P, SV or P-SV,	P,SV or P-SV,	Pure mode
Inversion	Dix-type differentiation	Dix-type differentiation	Linear layer stripping
Advantages	Converted wave	Converted wave	High accuracy, cusp and kink,
Limitation	Vertical velocity, high quality far-offset data	Vertical velocity, high quality far-offset data	Vertical velocity, high quality far-offset data, pure mode

2.6.3 A comparison of DMO inversion and Alkhalifah's inversion methods

Using the DMO inversion method, we can estimate vertical variations of η (Alkhalifah, 1997b). The DMO inversion method is probably more stable in inverting for the anisotropy parameters than is the Alkhalifah's inversion method, especially in the absence of large offsets and at later times (deeper targets), at which $x_{\max}/z$ is small (Alkhalifah, 1997b).

Unlike the DMO method, however, the Alkhalifah's inversion method does not require dipping reflectors and therefore is more flexible and can be applied to a broader range of field data. Moreover, it provides more opportunity to obtain lateral variations in η. For example, statistical estimation of lateral variations in η can be made from data at many common-midpoint (CMP) locations.

The Alkhalifah's moveout method can be used in the presence of very steep (nearly vertical) reflectors, such as on the flanks of salt domes where, in addition, reflections from interfaces with intermediate dips may not be available. Alkhalifah and Tsvankin (1995) showed that the DMO method fails to yield accurate values of η for such steep dips, primarily because the moveout for such reflections in TI media is not distinguishable from that in isotropic media or in any other anisotropic model. This Alkhalifah's inversion method, however, is based on the assumption of lateral homogeneity. Therefore, strong lateral inhomogeneities will cause problems for the method.

Table 2.3 summarizes the comparison of DMO inversion and Alkhalifah's inversion methods.

Table 2.3 A comparison of DMO inversion and Alkhalifah's inversion methods.

	DMO inversion	Alkhalifah's methods
VTI media	Weak	Weak
Spread	$X<Z$	$X>1.5Z$ for P-wave
Data	Surface	Surface
Wave mode	P wave	P wave
Inversion	Dix-type differentiation	Dix-type differentiation
Advantages	Stable	Flexible, steep dip reflectors
Limitation	Fails for steep dip reflectors	Vertical velocity, high quality far-offset data

CHAPTER 3: ANISOTROPIC MOVEOUT VELOCITY ANALYSIS METHODS FOR ESTIMATING THOMSEN'S ANISOTROPY PARAMETERS FROM P-WAVE MOVEOUT IN VTI LAYERS

The goal of geophysics is to determine the properties of the earth's interior from measurements on the surface and/or from boreholes. How do we determine subsurface structure and rock properties from these measurements? This problem of deriving properties of the earth—or creating a model of the earth—from the observed geophysical data constitutes an inverse problem. First, to understand how the data will be manipulated by the model, we must be able to calculate theoretical data for an assumed earth model. This constitutes the forward problem, which involves deriving a mathematical relationship between data and model. Figure 3.1 illustrates the difference in wavefront on a depth section for varying anisotropy parameters. These wavefronts are defined at a specific time, and represent the phase velocity at a specific angle. Figure 3.1(a) shows a fixed $\varepsilon = 0.2$ with varying δ = -0.6 to 0.6, and (b) a fixed δ = -0.2 with varying ε = -0.4 to 0.6. The inverse problem focuses on finding the solutions to these equations. In this chapter, anisotropy moveout velocity analysis methods, which include hyperbolic moveout velocity analysis, shifted hyperbolic moveout velocity analysis, modified three-term Taylor-series moveout velocity analysis and Alkhalifah's moveout velocity analysis, are investigated and compared in details. The reflection-traveltime approximations of the four respective anisotropy moveout velocity analysis equations to true traveltime, and their approaches for estimation of Thomsen's anisotropy parameters in layered anisotropic media are discussed.

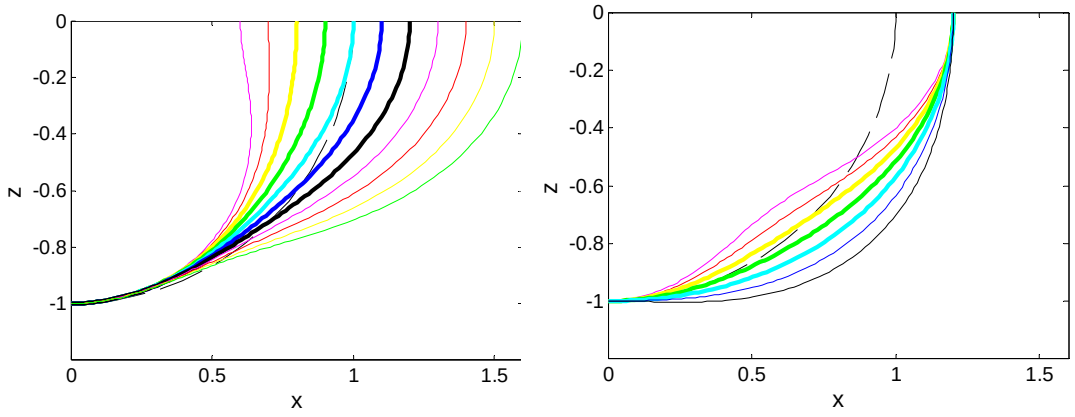

(a) (b)

Figure 3.1 Wavefronts on a depth section for varying anisotropy values, a) ε = 0.2 with varying δ = -0.6 to 0.6, and (b) δ = -0.2 with varying ε = -0.4 to 0.6.

3.1 Formulations for estimations of Thomsen's anisotropy parameters in layered anisotropic media

3.1.1 Hyperbolic estimates

As noted above, when one of two vertical velocities is known (by check shot or well log), we can estimate anisotropy parameters by obtaining the hyperbolic moveout velocity from seismic data. Although P- and SV-wave moveout in a transversely isotropic layer is generally nonhyperbolic, it usually remains close to hyperbolic for short-spread data (Tsvankin and Thomsen, 1994). Hence, as with an isotropic layer, NMO velocities for three waves (P-, SV- and SH-waves) can be obtained by hyperbolic approximation of traveltime. Unlike an isotropic layer, the short-spread moveout velocities for all three waves are generally different from the true vertical velocity in a single, horizontal, transversely isotropic layer. The P-wave short-spread moveout velocity is close to the vertical velocity (Winterstein, 1986). The SV-wave short-spread moveout velocity is

more significantly distorted by anisotropy than the P-wave velocity (Tsvankin and Thomsen, 1994). The SH-wave short-spread moveout velocity is equal to the horizontal velocity (Hake et al., 1984).

The SV-wave short-spread moveout velocity is determined by the parameter $\sigma = (\alpha_0 / \beta_0)^2 (\varepsilon - \delta)$. ε and δ almost always differ with $\varepsilon > \delta$ in most cases (Thomsen, 1986). So the character of the SV-wave moveout is strongly dependent on the sign of σ . If $\sigma > 0$ (the most common case), the SV-wave short-spread moveout remains close to hyperbolic whereas the SV-wave moveout for short-spread, as shown in Figure 3.2, can become strongly nonhyperbolic if $\sigma < 0$ (Tsvankin and Thomsen, 1994).

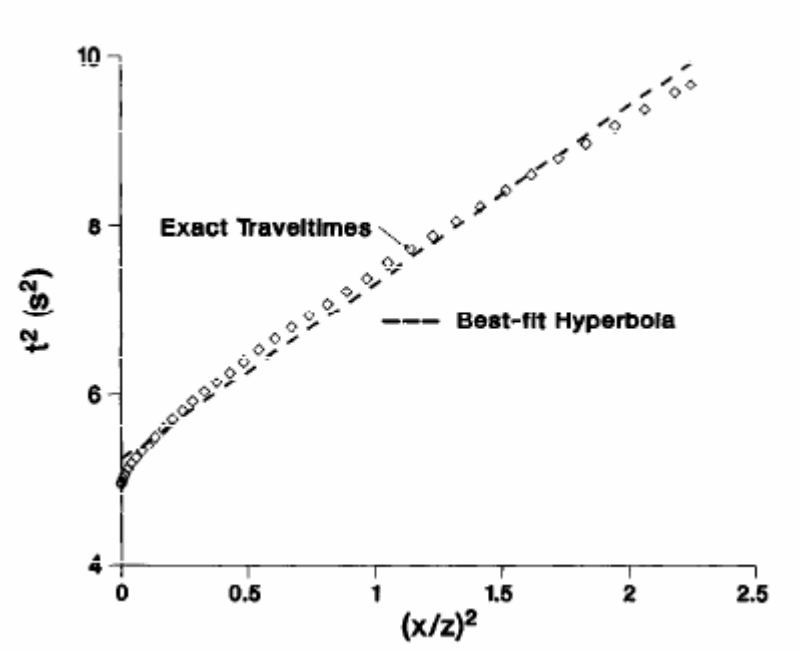

Figure 3.2 SV-wave moveout with negative σ for the model of Mesaverde mudshale from Levin (1989): $\alpha_0 = 4.529$ km/s, $\beta_0 = 2.703$ km/s, $\varepsilon = 0.034$, $\delta = 0.211 (\sigma = -0.497, 1 + 2\sigma = 0.006)$, $z = 3$ km. (After Tsvankin and Thomsen, 1994)

Tsvankin and Thomsen (1994) also pointed out that the P-SV wave does not exhibit the same anomalous nonhyperbolic moveout at very small offsets for $\sigma < 0$ as the SV-wave. Therefore, the short-offset P and P-SV moveouts usually can be used to recover the analytical value of the SV-wave short-offset moveout velocity.

Seriff and Sriram (1991), and Tsvankin and Thomsen (1994) define the short-spread moveout velocity for the converted P-SV wave as follows:

$$V_{\mathrm{NMO}}^2(\mathrm{P-SV}) = V_{\mathrm{NMO}}^2(\mathrm{P})\frac{t_{\mathrm{P0}}}{t_{\mathrm{P0}}+t_{\mathrm{S0}}} + V_{\mathrm{NMO}}^2(\mathrm{SV})\frac{t_{\mathrm{S0}}}{t_{\mathrm{P0}}+t_{\mathrm{S0}}}, \tag{3.1}$$

where $t_{\mathrm{p0}}, t_{\mathrm{s0}}$ are the two way vertical traveltimes for P-wave and P-SV converted waves, respectively.

3.1.2 Shifted hyperbolic estimates

As we know, a hyperbolic equation is defined by

$$t_{\mathrm{h}}^2 = t_0^2 + \frac{x^2}{V_{\mathrm{NMO}}^2}. \tag{3.2}$$

Castle (1994) shows that a time-shifted hyperbolic equation as follows:

$$\left(t_{\mathrm{sh}} - \tau_s\right)^2 = \left(t_0 - \tau_s\right)^2 + \frac{x^2}{V_{\mathrm{sh}}^2}. \tag{3.3}$$

Figure 3.3 shows the geometry of a hyperbolic NMO equation and the shifted hyperbola NMO equation. In this Figure, a red non-hyperbolic curve represents the offset

traveltimes for a horizontally layered earth, a blue curve is hyperbolic relative to the surface at $t = 0$, and a black curve is hyperbolic relative to the dashed horizontal time at time $t = \tau_s$ which is referred to as a shifted hyperbolic curve. The normal moveout velocity at zero offset is V_{NMO}, and the source-receiver offset is x.

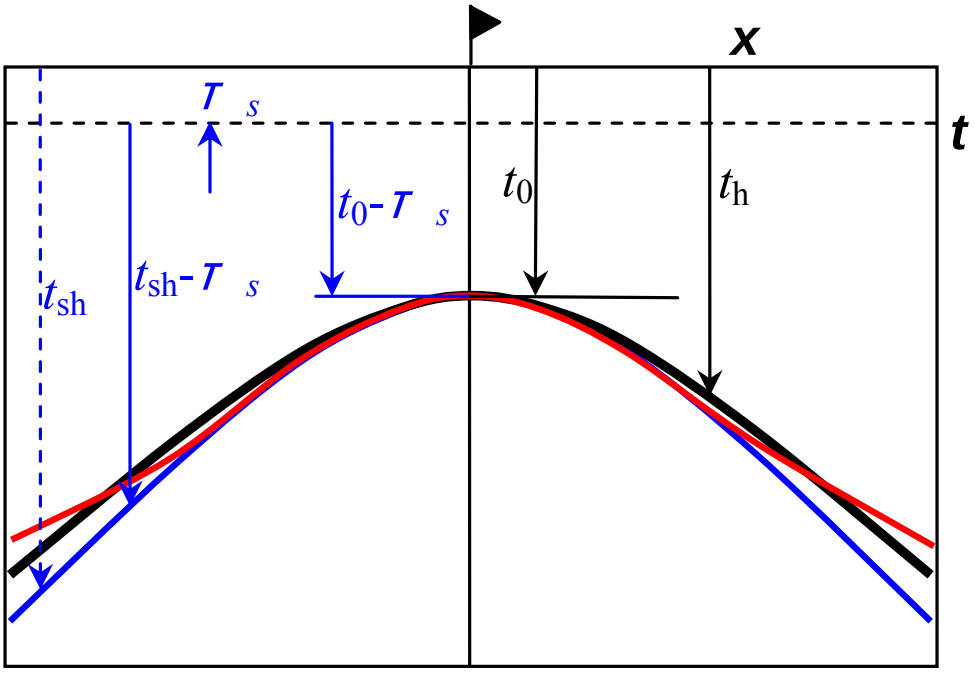

Figure 3.3 Geometry of a hyperbolic NMO equation and the shifted hyperbola NMO equation. (After John Bancroft, private communication)

Let $S = \dfrac{t_0}{t_0 - \tau_s}$, we can prove $V_{\mathrm{sh}}^2 = \dfrac{t_0 V_{\mathrm{NMO}}^2}{(t_0 - \tau_s)} = S V_{\mathrm{NMO}}^2$ (see Appendix A), which is substituted into Equation (3.3) so that we get

$$t = t_0\left(1 - \frac{1}{S}\right) + \sqrt{\left(\frac{t_0}{S}\right)^2 + \frac{x^2}{S V_{\mathrm{NMO}}^2}}\,. \tag{3.4}$$

Equation (3.4) is an exact equivalent of the fourth-order moveout equation. The equation may be expressed as,

$$t^2 = t_0^2 + \frac{x^2}{V_{NMO}^2} + \frac{1}{4}\frac{(1-S)x^4}{t_0^2 V_{NMO}^4}, \tag{3.5}$$

where

$$S = 1 + \frac{8(\varepsilon - \delta)(1 + 2\delta/(1 - \beta_0^2/\alpha_0^2))}{(1+2\delta)^2}. \tag{3.6}$$

When $S = 1$, Equation (3.5) reduces to the hyperbolic equation.

If we ignore the effect of shear wave on P wave, i.e. $\beta_0 = 0$,

$$S = 1 + \frac{8(\varepsilon - \delta)}{(1+2\delta)}. \tag{3.7}$$

3.1.3 Modified three-term Taylor series estimates

If the offset of a source and a receiver is larger than the depth of the reflector of interest, the nonhyperbolic moveout for P- and SV-waves can be observed in a single-layer model (Figure 3.4).

As can be seen from Figure 3.4, the error of the hyperbolic approximation for both P and SV waves rapidly grows for $x_{\max} > z$ and the residual moveout for the long-offset SV-wave after the hyperbolic correction is higher than that for the long-offset P-wave. This demonstrates that the long-offset SV moveout has higher sensitivity to anisotropy parameters than the long-offset P moveout. This also means we should use higher order

Taylor series expansion to approximate the P- and SV-waves traveltimes and investigate the relationship between moveout velocities and parameters of anisotropy.

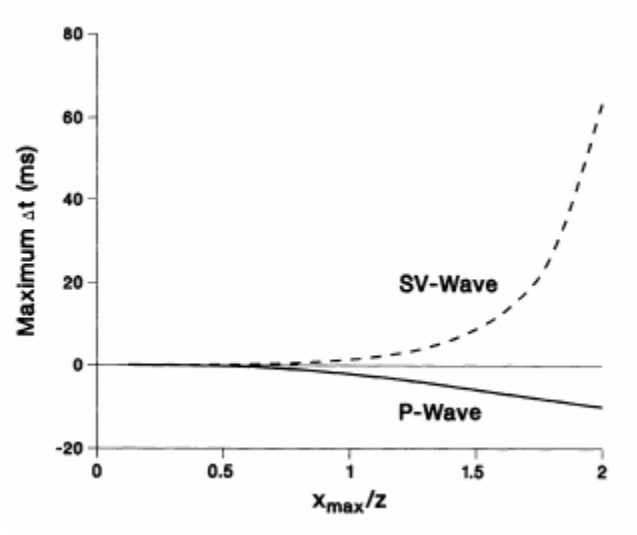

Figure 3.4 Maximum differences between the exact traveltimes and the best-fit hyperbola as a function of spread-length-to-depth ratio $x_{\max}/z$. The model is Taylor sandstone with $z = 3$ km. (After Tsvankin and Thomsen, 1994)

There are many analytic descriptions of traveltime curves for long-offset P- and SV-waves. A popular approach for estimating anisotropy is a three-term Taylor series approximation to the reflection moveout curve (Taner and Koehler, 1969; Hake et al, 1984; Tsvankin and Thomsen, 1994):

$$t^2 = A_0 + A_2 x^2 + A_4 x^4 + \cdots \tag{3.8}$$

$$A_0 = t_0^2,\ A_2 = \frac{\mathrm{d}\left(t^2\right)}{\mathrm{d}\left(x^2\right)}\bigg|_{x=0},\ A_4 = \frac{1}{2}\frac{\mathrm{d}}{\mathrm{d}\left(x^2\right)}\left(\frac{\mathrm{d}\left(t^2\right)}{\mathrm{d}\left(x^2\right)}\right)\bigg|_{x=0},$$

where t_0 is the true zero-offset arrival time; t is the x-offset arrival time; A_0, A_2 and A_4 are the coefficients of Taylor series and the higher order terms (A_4 and up) which describe nonhyperbolic moveout for larger offsets due to the presence of anisotropy and/or vertical heterogeneities.

Taylor-series coefficients in a single layer with weak anisotropy

Tsvankin and Thomsen (1994) derive the following expression for reflection moveouts of the P- and SV-wave in a single layer at the limit of weak anisotropy:

$$t^2 = t_0^2 + A_2 x^2 + \frac{A_4 x^4}{1 + \left(\frac{x}{v_0 t_0} \right)^2}, \tag{3.9}$$

where v_0 is the vertical velocity for P- and SV-waves and the parameters A_2 and A_4 are Taylor-series coefficients from Equation (3.8) within the limits of weak anisotropy.

For the P-wave,

$$A_2(\mathrm{P}) = \frac{1 - 2\delta}{\alpha_0^2}, \tag{3.10a}$$

$$A_4(\mathrm{P}) = -\frac{2(\varepsilon - \delta)}{t_{P0}^2 \alpha_0^4}, \tag{3.10b}$$

and, for the SV-wave,

$$A_2(\mathrm{SV}) = \frac{1 - 2\sigma}{\beta_0^2}, \tag{3.11a}$$

$$A_4(\mathrm{SV}) = \frac{2\sigma}{t_{S0}^2 \beta_0^4} = -\left(\frac{\alpha_0}{\beta_0}\right)^4 A_4(\mathrm{P}). \tag{3.11b}$$

Byun et al. (1989) and Byun and Corrigan (1990) presented the so-called "skewed" hyperbolic moveout equation for long-offset P-wave moveout also based on Thomsen's formulae for weak anisotropic media:

For surface seismic data,

$$t^2 = t_0^2 + \left[t_0^2 (V_{\mathrm{v}} / V_{\gamma})^2 + x^2 / V_{\mathrm{h}}^2\right] \frac{x^2}{x^2 + t_0^2 V_{\mathrm{v}}^2}. \tag{3.12a}$$

For VSP geometry,

$$t^2 = \frac{z^2}{V_{\mathrm{v}}^2} + \left[\frac{z^2}{V_{\gamma}^2} + \frac{z^2}{V_{\mathrm{h}}^2}\right] \frac{x^2}{x^2 + z^2}, \tag{3.12b}$$

where z is depth; t_0 is the vertical traveltime; V_{v} is the average vertical velocity and V_{h} and V_{γ} are defined as the horizontal and skew moveout velocities, respectively, which can be found by least squares or by a semblance analysis.

Sena (1991) derived analytical expressions for the parameters of Equation (3.12) under the assumption of weak anisotropy. The quartic Taylor-series coefficient for a single-layer model was given by Sena (in the present notation) as

$$A_4(\mathrm{P}) = -\frac{2(\varepsilon - \delta)}{t_{P0}^2 \alpha_0^4} \frac{1}{(1 + 2\varepsilon)(1 + 2\delta)}. \tag{3.13}$$

Note that Equations (3.9) through (3.13) are valid only for weak anisotropy.

As Tsvankin and Thomsen (1994) note, concise analytic expressions for traveltime curves in transversely isotropic media cannot be obtained without assumptions such as weak or elliptical anisotropy. Under the assumption of small angles (i.e. near the vertical), Tsvankin and Thomsen (1994) analyzed the three-term Taylor series with coefficients valid for arbitrary transverse isotropy. Parameters A_2 and A_4 for a single layer is:

$$A_2(\mathrm{P}) = \frac{1}{V_{\mathrm{NMO}}^2(\mathrm{P})} = \frac{1}{\alpha_0^2(1+2\delta)}, \tag{3.14a}$$

$$A_4(\mathrm{P}) = -\frac{2(\varepsilon-\delta)}{t_{P0}^2\alpha_0^4}\frac{1+\dfrac{2\delta}{1-\beta_0^2/\alpha_0^2}}{(1+2\delta)^4}, \tag{3.14b}$$

$$A_2(\mathrm{SV}) = \frac{1}{V_{\mathrm{NMO}}^2(\mathrm{SV})} = \frac{1}{\beta_0^2(1+2\sigma)}, \tag{3.15a}$$

$$A_4(\mathrm{SV}) = \frac{2\sigma}{t_{S0}^2\beta_0^4}\frac{1+\dfrac{2\delta}{1-\beta_0^2/\alpha_0^2}}{(1+2\sigma)^4}. \tag{3.15b}$$

Unfortunately, for long spreads ($x_{\max}/z > 2$), the three-term Taylor series expansion is not accurate because the moveout velocity of the traveltime curves does not converge to the horizontal velocity. Hence, Tsvankin and Thomsen (1994) proposed replacing A_4 by A_4', given by

$$A_4' = \frac{A_4}{1 + Ax^2}, \tag{3.16}$$

where

$$A = \frac{A_4}{V_{\mathrm{h}}^{-2} - A_2}. \tag{3.17}$$

We have the following approximated expression for reflection moveouts in a single layer:

$$t_A^2 = t_0^2 + A_2 x^2 + \frac{A_4 x^4}{1 + Ax^2}. \tag{3.18}$$

For P-waves, Equation (3.18) provides an excellent fit to the exact traveltime, even for long spreads and substantial anisotropy, as illustrated in Figure 3.5. For SV-waves, the area of validity for approximation is much more limited, as illustrated in Figure 3.6.

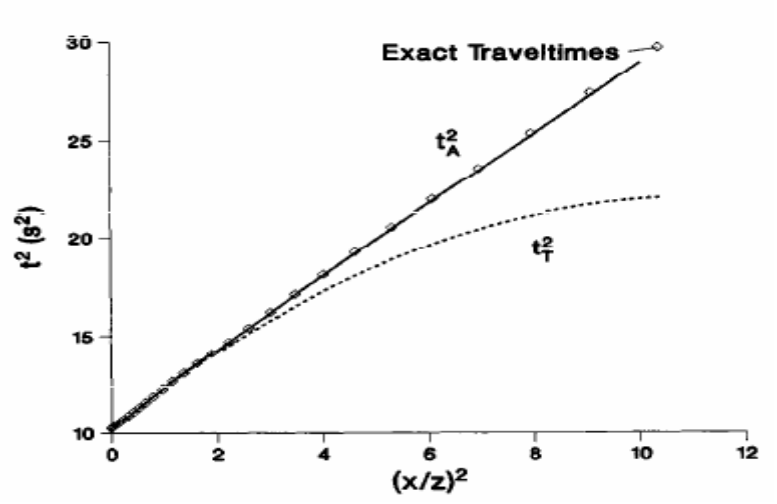

Figure 3.5 Three term Taylor series t_{T} and approximation t_{A} for P-wave moveout in a layer of Dog Creek shale with z=3 km. (After Tsvankin and Thomsen, 1994)

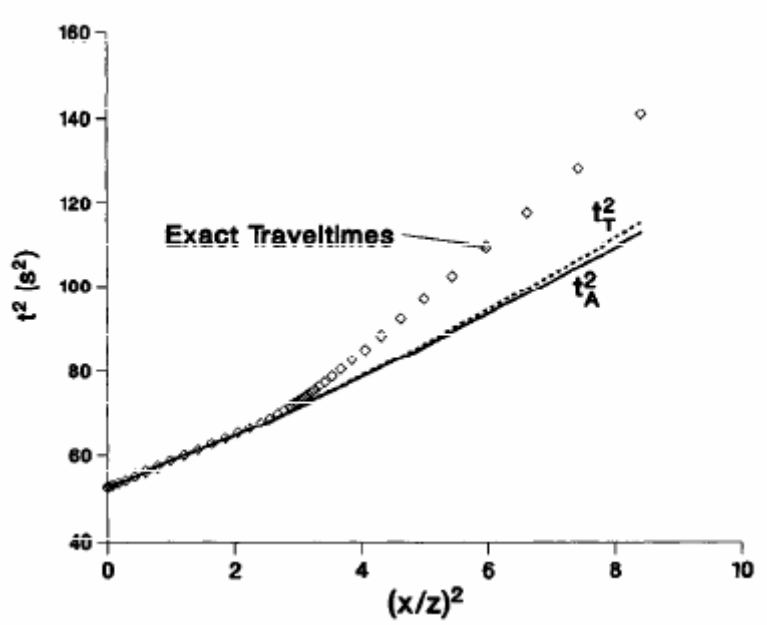

Figure 3.6 Three term Taylor series t_{T} and approximation t_{A} for SV-wave moveout in a layer of Dog Creek shale with $z = 3$ km. (After Tsvankin and Thomsen, 1994)

3.1.4 Alkhalifah's estimates

If one ignores the contribution of the vertical shear-wave velocity, a modified three-term Taylor-series approximation to the reflection moveout curve can be fully determined by two parameters, V_{NMO} (NMO velocity) and η $[= (\varepsilon - \delta)/(1 + 2\delta)$ (Alkhalifah and Tsvankin, 1995), or by V_{NMO} and V_{h} (horizontal velocity).

$$t^2(x) = t_0^2 + \frac{x^2}{V_{\mathrm{NMO}}^2} - \frac{\left(V_{\mathrm{h}}^2 - V_{\mathrm{NMO}}^2\right)x^4}{V_{\mathrm{NMO}}^2\left(t_0^2 V_{\mathrm{NMO}}^4 + V_{\mathrm{h}}^2 x^2\right)}. \tag{3.19}$$

This is the so-called Alkhalifah's anisotropy moveout velocity analysis method.

3.1.5 Estimates in multilayered media

a) Moveout velocity in multilayered media

For a medium with N homogeneous, coarse, constant velocity layers, the short-spread moveout velocity is given by (Hake et al., 1984; Tsvankin and Thomsen, 1994):

$$V_{\mathrm{NMO}}^2(\mathrm{P,SV}) = \lim_{x\to 0}\frac{\mathrm{d}\left(x^2\right)}{\mathrm{d}\left(t^2\right)}(\mathrm{P,SV}) = \frac{1}{t_0(N)}\sum_{i=1}^{N} v_{\mathrm{nmo,i}}^2 \Delta t_{0i}\,, \tag{3.20}$$

where $v_{nmo,i}$ is the interval NMO velocity for P-P or SV-SV waves in layer i, which may be recovered using the short-spread NMO velocities $V_{\mathrm{NMO}}^2(P,SV)$ for the reflections from the top and bottom of the layer; $t_0(N)$ is the two-way vertical traveltime to the bottom of layer N and Δt_{0i} is the two-way vertical traveltime in layer i.

Substituting Equation (2.22) into equation (3.20), we have

$$V_{\mathrm{NMO}}^2(\mathrm{P,SV\ or\ SH}) = \frac{1}{t_0(N)}\sum_{i=1}^{N} v_{0i}^2(1+\zeta_i)\Delta t_i = \frac{1}{t_0(N)}\sum_{i=1}^{N} v_{0i}^2 \Delta t_i + \frac{1}{t_0(N)}\sum_{i=1}^{N} v_{0i}^2 \zeta_i \Delta t_i$$

$$= V_{\mathrm{RMS}}^2(N) + \frac{1}{t_0(N)}\sum_{i=1}^{N} v_{0i}^2 \zeta_i \Delta t_i\,, \tag{3.21}$$

where ζ_i stands for anisotropy parameters δ_i, σ_i, or γ_i for the P-, SV-, or SH-wave in layer i, respectively; v_{0i} stands for α_0 for P-wave, β_0 for SV- or SH-waves in layer i; and $V_{\mathrm{RMS}}(N)$ is the vertical RMS velocity, which may be obtained by check shot or well log. From Equation (3.21), we have

$$V_{\mathrm{NMO}}^2(N) = V_{\mathrm{RMS}}^2(N) + \frac{1}{t_0(N)} \sum_{i=1}^{N} v_{0i}^2 \zeta_i \Delta t_i \,, \tag{3.22a}$$

$$V_{\mathrm{NMO}}^2(N-1) = V_{\mathrm{RMS}}^2(N-1) + \frac{1}{t_0(N-1)} \sum_{i=1}^{N-1} v_{0i}^2 \zeta_i \Delta t_i \;\; . \tag{3.22b}$$

Thus,

$$\zeta_N = \frac{\left(V_{\mathrm{NMO}}^2(N) - V_{\mathrm{RMS}}^2(N)\right)\, t_0(N) - \left(V_{\mathrm{NMO}}^2(N-1) - V_{\mathrm{RMS}}^2(N-1)\right)\, t_0(N-1)}{v_{0N}^2 \left(t_0(N) - t_0(N-1)\right)}, \tag{3.23}$$

where

$$v_{0N}^2 = \frac{\left(V_{\mathrm{RMS}}^2(N)\right)\, t_0(N) - \left(V_{\mathrm{RMS}}^2(N-1)\right)\, t_0(N-1)}{\left(t_0(N) - t_0(N-1)\right)}. \tag{3.24}$$

b) Effective coefficients in multilayered media

For multilayered media, the coefficient A_4 for pure modes is given by (Hake et al., 1984; Tsvankin and Thomsen, 1994)

$$A_4(\mathrm{P,SV,or\ \ SH}) = \frac{\left(\sum_{i=1}^{N} v_{\mathrm{nmo},i}^2 \Delta t_{0i}\right)^2 - t_0(N)\sum_{i=1}^{N} v_{\mathrm{nmo},i}^4 \Delta t_{0i}}{4\left(\sum_{i=1}^{N} v_{\mathrm{nmo},i}^2 \Delta t_{0i}\right)^4} + \frac{t_0(N)\sum_{i=1}^{N} A_{4i} v_{\mathrm{nmo},i}^8 \Delta t_{0i}^3}{\left(\sum_{i=1}^{N} v_{\mathrm{nmo},i}^2 \Delta t_{0i}\right)^4}, \quad (3.25)$$

where A_{4i} is the quartic coefficient for layer i; $v_{\mathrm{nmo},i}$ is the interval NMO velocity for P-P or SV-SV waves in layer i, which may be recovered similarly using the short-spread moveout velocities $V_{\mathrm{NMO}}^2(\mathrm{P,SV})$ for the reflections from the top and bottom of the layer; $t_0(N)$ is the two-way vertical traveltime to the bottom of the layer N, and Δt_{0i} is the two-way vertical traveltime in layer i.

Since

$$V_{\mathrm{NMO}}^2(\mathrm{P,SV}) = \frac{1}{A_2(\mathrm{P,SV})} = \lim_{x\to 0} \frac{\mathrm{d}\left(x^2\right)}{\mathrm{d}\left(t^2\right)}(\mathrm{P,S}V) = \frac{1}{t_0(N)} \sum_{i=1}^{N} v_{\mathrm{nmo},i}^2 \Delta t_{0i}, \quad (3.26)$$

Equation (3.25) may be rearranged using Equation (3.26) as:

$$\frac{1}{t_0(N)} \sum_{i=1}^{N} \left(v_{\mathrm{nmo},i}^4 + H_i\right) \Delta t_{0i} = V_{\mathrm{NMO}}^4(N)\left(1 - 4A_4(N) t_0^2(N) V_{\mathrm{NMO}}^4(N)\right), \quad (3.27)$$

where

$$H_i = -4A_{4i}t_0^2 v_{\text{nmo},i}^8 . \tag{3.28}$$

Let

$$F(N) = V_{\text{NMO}}^4(N)\left(1 - 4A_4(N)t_0^2(N)V_{\text{NMO}}^4(N)\right), \tag{3.29}$$

$F(N)$ is thus a known function of the Taylor-series coefficients for the reflection from the N th interface. Having found $F(N)$ and $F(N-1)$ using the reflections from the top and bottom of the N th layer, we may obtain

$$H_N = \frac{F(N)t_0(N) - F(N-1)t_0(N-1)}{t_0(N) - t_0(N-1)} - v_{\text{nmo},i}^4 , \tag{3.30}$$

where

$$H_N = -4A_{4N}t_0^2 v_{\text{nmo},N}^8 , \tag{3.31}$$

$$v_{\text{nmo},N}^2 = \frac{V_{\text{NMO}}^2(N)t_0(N) - V_{\text{NMO}}^2(N-1)t_0(N-1)}{t_0(N) - t_0(N-1)} . \tag{3.32}$$

Equations (3.14), (3.15) and (3.25) are valid for arbitrary transverse isotropy (Tsvankin and Thomsen, 1995).

3.2 Reflection-traveltime approximations of four moveout equations to true traveltime in layered anisotropic media

The traveltimes for reflected seismic waves is of primary importance to most

processing and interpretation algorithms. In order to make qualitative estimates of the influence of anisotropy on seismic reflection-traveltime and to develop inversion algorithms for anisotropic media, it is very important to understand the relationships between approximated reflection-traveltime and true traveltime as well as the effects of the medium parameters and spread length.

The P-wave traveltime approximations for four reflection-traveltime inversion methods are given as follows.

1) The hyperbolic reflection-traveltime approximation:

$$t^2(x) = t_0^2 + \frac{x^2}{V_{\mathrm{NMO}}^2}, \tag{3.33}$$

2) The modified three-term Taylor-series approximations (Tsvankin and Thomsen, 1994) of the limit of weak anisotropy:

$$t^2(x) = t_0^2 + \frac{x^2}{V_{\mathrm{NMO}}^2} + \frac{A_4 x^4}{1 + \left(\frac{x}{\alpha_0 t_0}\right)^2}; \tag{3.34}$$

3) The shifted-hyperbolic approximation (Castle, 1994):

$$t(x) = \tau_s + \sqrt{\tau_x^2 + \frac{x^2}{SV_{\mathrm{NMO}}^2}}\ ; \tag{3.35}$$

4) The Alkhalifah's approximation (Tsvankin and Thomsen, 1994):

$$t^2(x) = t_0^2 + \frac{x^2}{V_{\mathrm{NMO}}^2} - \frac{\left(V_{\mathrm{h}}^2 - V_{\mathrm{NMO}}^2\right)x^4}{V_{\mathrm{NMO}}^2\left(t_0^2 V_{\mathrm{NMO}}^4 + V_{\mathrm{h}}^2 x^2\right)}. \tag{3.36}$$

From Equation (3.33) to Equation (3.36), for a single transversely isotropic layer,

$$V_{\mathrm{NMO}}^2(P) = \alpha_0^2(1+2\delta)\ , V_{\mathrm{h}}^2 = \alpha_0^2(1+2\varepsilon), \tag{3.37}$$

$$A_4(P) = -\frac{2(\varepsilon-\delta)}{t_0^2\alpha_0^4}, \tag{3.38}$$

$$\tau_s = t_0\left(1-\frac{1}{S}\right), \tau_x = \frac{t_0}{S},\ S = 1+\frac{8(\varepsilon-\delta)}{(1+2\delta)}, \tag{3.39}$$

where α_0 is the vertical velocity for P waves, β_0 is the vertical SV-wave velocity, δ and ε are Thomsen's anisotropy parameters; V_{NMO} is NMO velocity, V_{h} is horizontal velocity for P-waves, t_0 and t are the two-way traveltimes for zero-offset and offset x, respectively, and S is the shift parameter.

Using an approximation of the exact eikonal equation in the quasi-compressional case for so-called weak anisotropy (Daley, 2001) and the relationships between phase and group velocity (Thomsen, 1986), we develop multilayer ray-tracing code for modelling real traveltime-offset curves (blue solid line shown in Figure 3.7). To gain insight on the influence of transverse isotropy on seismic signatures, we applied the weak-anisotropy approximation systematically and checked its accuracy by comparing it with the exact solutions from ray-tracing.

We use these formulae (3.33) to (3.36) as the basis for semblance analysis or mean-square fitting to see how well these formulae work for both small and large offsets.

3.2.1 Approximations versus offset range

Figure 3.7 demonstrates all four approximations to the exact reflection traveltime at an offset/depth of 2.0. As can be seen: 1) The hyperbolic approximates the exact reflection traveltime over a short offset range (offset/depth ≈ 0.5); 2) The modified three-term Taylor series and the shifted hyperbolic approximate the exact reflection traveltime over middle offset ranges (offset/depth ≈ 1.0 for the modified three-term Taylor series, and offset/depth ≈ 1.5 for the shifted hyperbolic); 3) The Alkhalifah's approximates the exact reflection traveltime over a long offset range (offset/depth ≈ 2.0). This demonstrates that each traveltime approximation has its own offset range. The ranges of the offset (a ratio of offsets and depth) are about 0.5, 1.0, 1.5, and 2.0 for the hyperbolic, Taylor, shifted hyperbolic, and Alkhalifah's approximations, respectively.

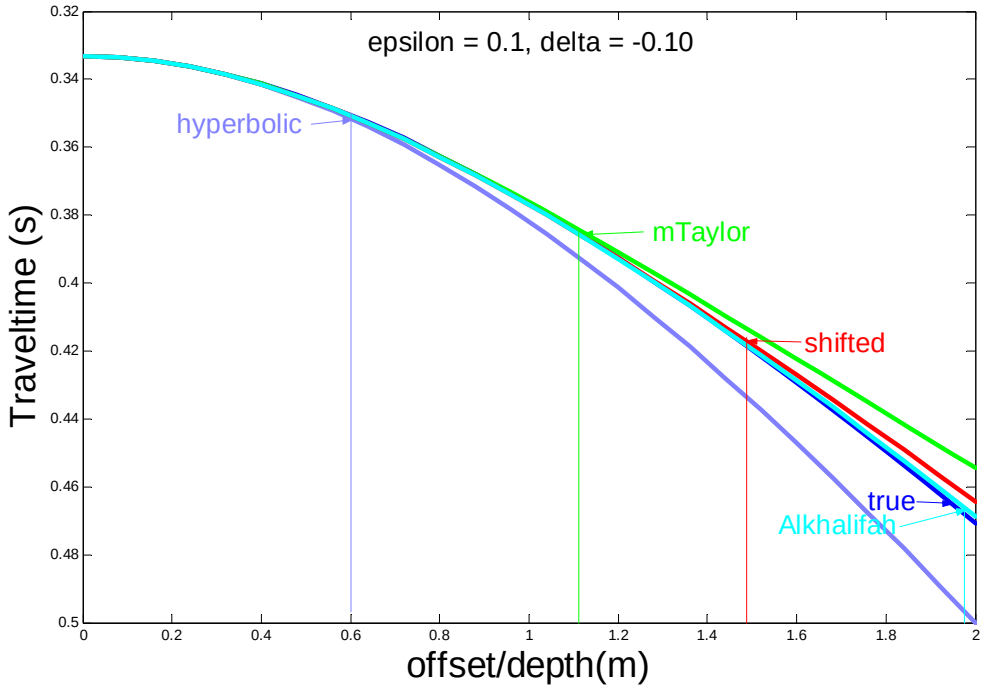

Figure 3.7 Reflection-traveltime approximations to true reflection traveltime under different offset ranges. Blue line: the exact traveltime; purple line: hyperbolic approximation; green line: the modified three-term Taylor-series approximation; red line: the shifted-hyperbolic approximation; cyan line: Alkhalifah's approximation.

3.2.2 Approximations versus anisotropy parameters

Figure 3.8 shows examples of all four approximations to the exact reflection traveltime under different anisotropy parameters. There the following can be seen: 1) When $\varepsilon - \delta = 0$ (elliptical anisotropy), the four approximations reduce to the exact traveltime (Figure 3.8a). 2) When $0 < \varepsilon - \delta \le 0.2$, all four closely approximate the exact traveltime for short spreads, but the hyperbolic and the modified three-term Taylor-series traveltimes deviate increasingly from the actual traveltime with increasing spread length (Figure 3.8b). 3) When $\varepsilon - \delta > 0.2$, both the shifted hyperbolic and Alkhalifah's

traveltimes approximate closely the actual reflection traveltime, the modified three-term Taylor-series approximation is quite poor, and the hyperbolic approximation deviates grossly from the

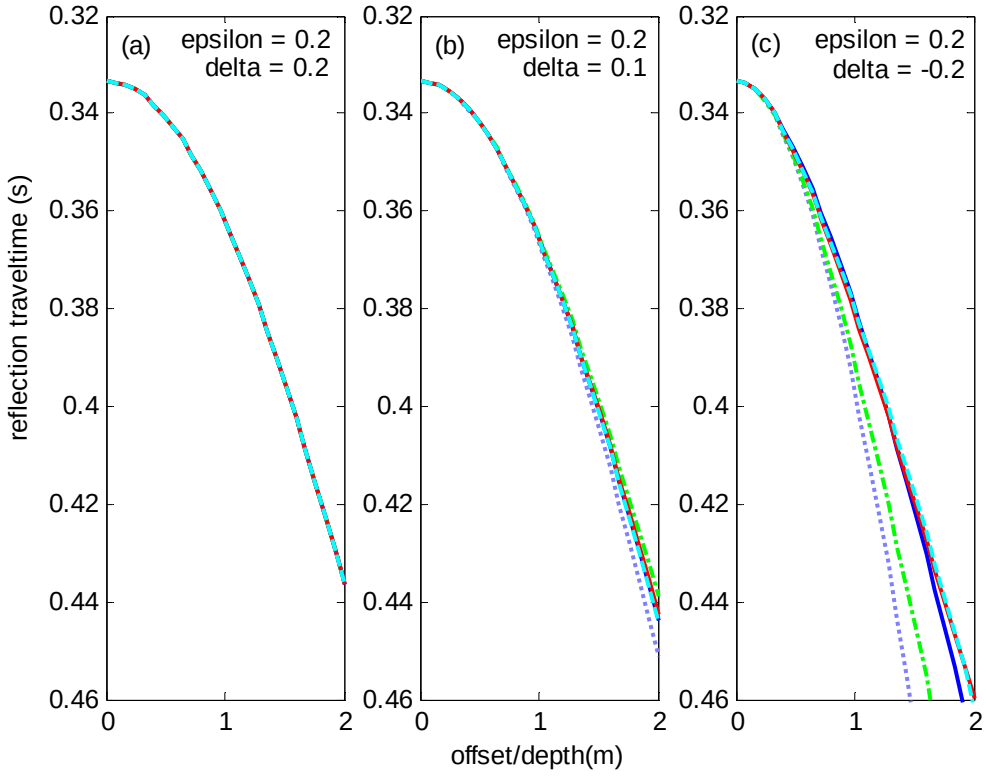

Figure 3.8 Reflection-traveltime approximations to true reflection traveltime under different anisotropy parameters. Solid blue line: the exact traveltime; purple dotted line: hyperbolic approximation; green dash-dot line: the modified three-term Taylor-series approximation; red solid line: the shifted-hyperbolic approximation; cyan dashed line: Alkhalifah's approximation.

actual reflection traveltime, even for a short spread (Figure 3.8c). This demonstrates that traveltime approximations also depend on anisotropy parameters.

3.2.3 Approximations versus vertical P-wave velocity

Figure 3.9 shows examples of all four approximations to the exact reflection traveltime under different vertical P-wave velocities. It can be seen that when estimated

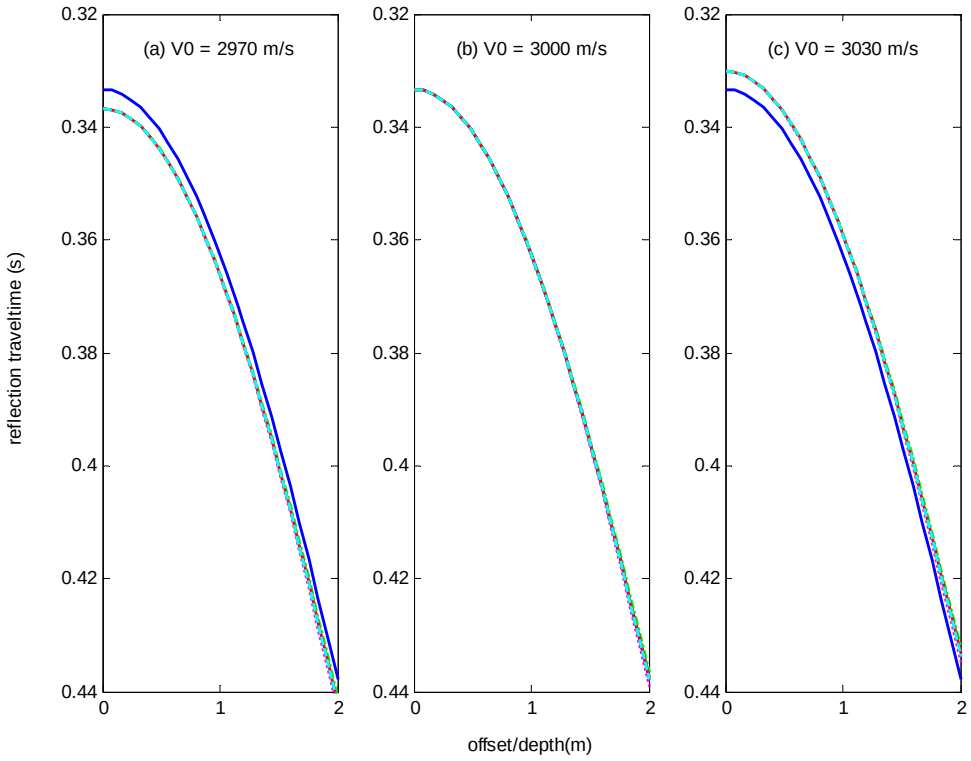

Figure 3.9 Reflection-traveltime approximations to true reflection traveltime under different vertical velocities. Solid blue line: the exact traveltime; purple dotted line: hyperbolic approximation; green dash-dot line: the modified three-term Taylor-series approximation; red solid line: the shifted-hyperbolic approximation; cyan dashed line: Alkhalifah's approximation.

vertical velocity is lower or higher than actual vertical velocity (3000 m/s), the four approximations behave the same and all depart from true traveltime. This also tells us

that vertical P-wave velocity is a key parameter in the estimation of anisotropy parameters.

3.2.4 Approximations versus zero-offset traveltime

Figure 3.10 shows examples of all four approximations to the exact reflection

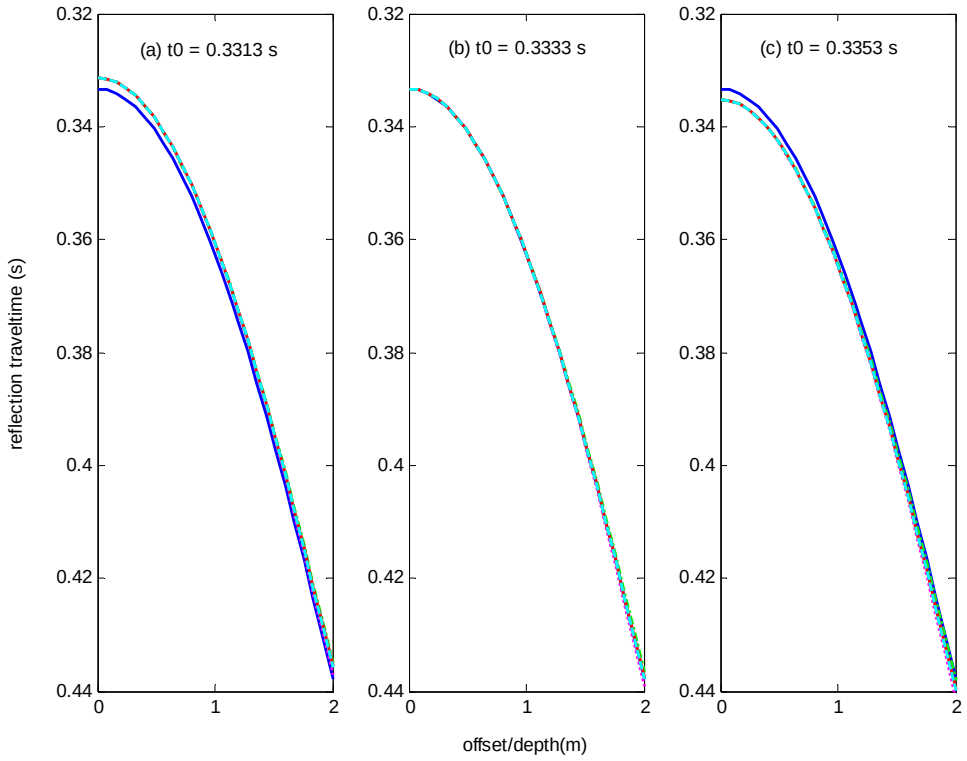

Figure 3.10 Reflection-traveltime approximations to true reflection traveltime under different zero-offset two-way traveltime. Solid blue line: the exact traveltime; purple dotted line: hyperbolic approximation; green dash-dot line: the modified three-term Taylor-series approximation; red solid line: the shifted-hyperbolic approximation; cyan dashed line: Alkhalifah's approximation.

traveltime under different zero-offset traveltime. It can be seen that when zero-offset traveltime is smaller or larger than actual zero-offset traveltime (0.3333s), the four approximations behave the same and all depart from true traveltime. This tells us that in estimating anisotropy parameters, the smaller the sampling rate, the better the estimated anisotropy parameters.

3.3 Approaches for estimating effective parameters in layered anisotropic media

Using Equations (3.33) to (3.36), we can pick up effective coefficients A_4, V_{NMO}, V_{h} and S, and then obtain anisotropy parameters ε and δ by using Equations (3.37) to (3.39) through a Dix-type differentiation procedure (here, vertical P-wave velocity α_0 is known from the well log).

3.3.1 Procedure for estimating Thomsen's anisotropy parameters

The main steps for estimating anisotropy parameters for P-wave are:

1. Find the moveout velocities $V_{\mathrm{NMO}}(N)$, $V_{\mathrm{NMO}}(N-1)$ and effective coefficients corresponding to the reflections from the top and the bottom of any particular layer.

2. Compute $V^2_{\mathrm{RMS}}(N)$ and $V^2_{\mathrm{RMS}}(N-1)$ from check shot or well log.

3. Apply the Dix-type formulas to recover the P-wave interval coefficients for layer i, in combination with the vertical arrival times.

4. The anisotropy parameters may be obtained by inverting the interval coefficients.

Least-square traveltime fitting or semblance analysis is employed to estimate effective coefficients.

3.3.2 Mean-square traveltime fitting

We have performed an extensive search in the model space to determine the behaviour of the objective function near the exact solution. The objective function for least-square traveltime fitting was defined as the rms value of time residual Δt calculated with respect to the exact traveltime curve (Tsvankin, et al, 1995),

$$\Delta t_{\text{rms}} = \sqrt{\frac{1}{M}\sum_{j=1}^{M}\Delta t_j^2} = \sqrt{\frac{1}{M}\sum_{j=1}^{M}(t_{\text{real}} - t_{\text{calculated}})_j^2}\ , \tag{3.40}$$

where the number of receivers is M , t_{real} is picked traveltime from CMP gather, and $t_{\text{calculated}}$ is calculated traveltime according to Equations (3.33), (3.34), (3.35) or (3.36). For each traveltime event, the model parameters were systematically varied, within a reasonable range, and a multidimensional objective function was constructed in the neighbourhood of the exact solution.

Figure 3.11 shows the mean-square traveltime fitting plots using the Alkhalifah's approximation. On Figure 3.11(a), x coordinates represent NMO velocities and y coordinates represent horizontal velocities. Values of Δt_{rms} were computed at each grid location and the contours of these traveltime are shown. The symbol o indicates the true values of V_{NMO} and V_{h} while + indicates the estimated values. The estimated values are

obtained by searching minimum Δt_{rms}. On Figure 3.11(b), the actual seismic arrival times (red) are plotted together with the traveltime curves (blue) calculated using the estimated velocities from Figure 3.11(a). The close fit of actual events with those calculated from the approximated velocities shows that mean-square traveltime fitting is capable of estimating traveltime quite well. It can also be seen from Figure 3.11 that the deviations of the estimated values from the true values are the result of the subsurface anisotropy parameters because $\varepsilon - \delta = 0.4 > 0.2$, which will be explained in Chapter 4.

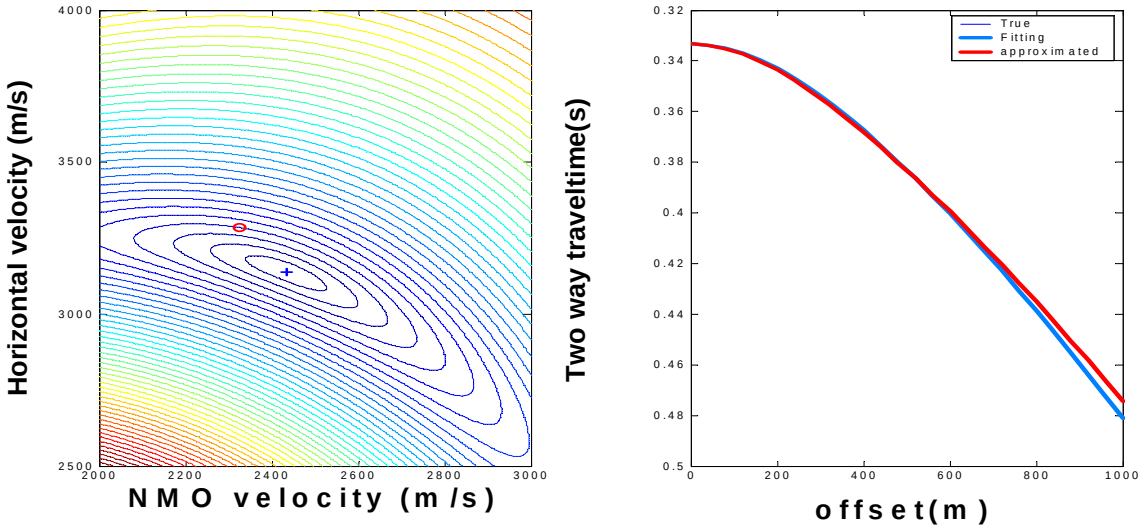

(a) (b)

Figure 3.11 The semblance plots using Alkhalifah's approximation for parameters: $\varepsilon = 0.2$, $\delta = -0.2$ with (a) Δt_{rms} contour; (b) traveltime versus offset.

3.3.3 Semblance analysis

Semblance analysis is less sensitive to traveltime errors than mean-square traveltime fitting and generally produces more stable results. The semblance coefficient is defined as the ratio of the output energy over a window of a stack of traces to the input energy in

the unstacked traces. In mathematical terms, S_k , the semblance coefficient (Neidell, N.S. et al, 1971) for *M* traces, is

$$S_k = \frac{\sum_{l=k-N/2}^{k+N/2} \left[\sum_{i=1}^{M} f_{i,j(i,l)} \right]^2}{M \sum_{l=k-N/2}^{k+N/2} \sum_{i=1}^{M} f_{i,j(i,l)}^2}, \tag{3.41}$$

where $f_{i,j(i,l)}$ is the amplitude in trace i at the time sample j which varies with the zero-offset time sample l and the trace (offset) i . The window size $N+1$, usually equal to the dominant period of the wavelet, is used to smooth the semblance spectrum estimates. The semblance coefficient has a maximum value of unity (when all traces are identical) and a minimum value of zero.

Figure 3.12 shows the semblance plots using the Alkhalifah's approximation. On the left side, the symbol o represents the true values of V_{NMO} and V_{h} while + represents the estimated values. On the right side, the actual seismic arrival times (red) are plotted together with the traveltime curves (blue) calculated using the estimated velocities from the left side. The close fit of actual events with those calculated from the approximated velocities shows that semblance analysis is capable of estimating traveltime quite well. It can also be seen from Figure 3.12c that the deviations of the estimated values from the true values depend on the subsurface anisotropy parameters because $\varepsilon - \delta = 0.4 > 0.2$, which will be explained in Chapter 4.

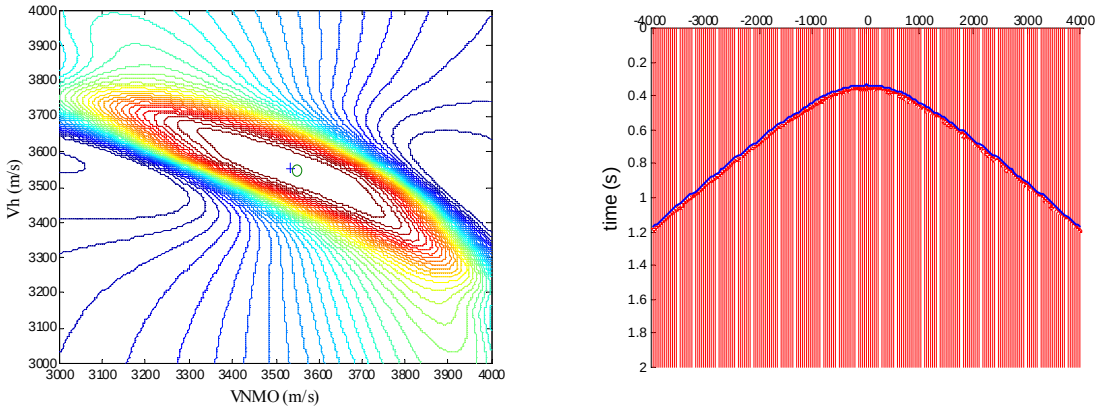

(a)

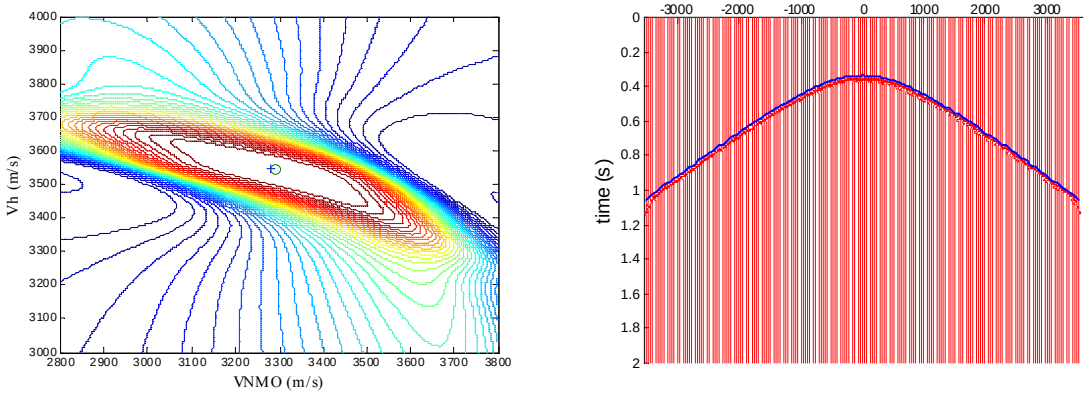

(b)

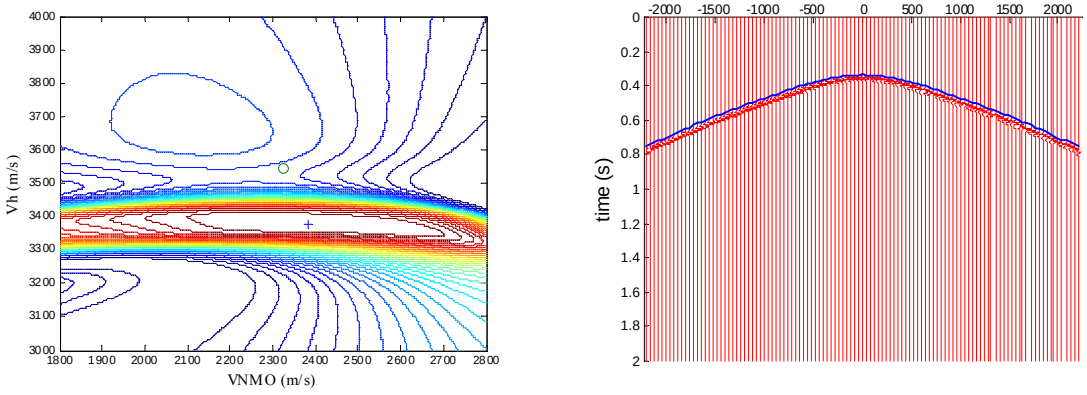

(c)

Figure 3.12 The semblance plots using Alkhalifah's approximation for anisotropy parameters: (a) $\varepsilon = 0.2$, $\delta = 0.2$; (b) $\varepsilon = 0.2$, $\delta = 0.1$; (c) $\varepsilon = 0.2$, $\delta = -0.2$.

CHAPTER 4: SYNTHETIC INVERSIONS OF P-WAVE MOVEOUTS IN VTI LAYERS

4.1. Single VTI layer over an isotropic layer

For simplicity, we consider a series of single-layer cases in order to determine how both actual anisotropy parameters and spread length affect the estimation of anisotropy parameters. The input CMP gather for anisotropy-parameter estimation contains a single reflection from a flat interface. The depth of this interface is 500 m. Vertical P- and S-wave velocities above the reflector are 3000 m/s and 1500 m/s, respectively. The values of ε are fixed at 0.2, 0.1 and 0.0, respectively, and those of δ range from –0.2 to 0.2 in increments of 0.02. (Figure 4.1)

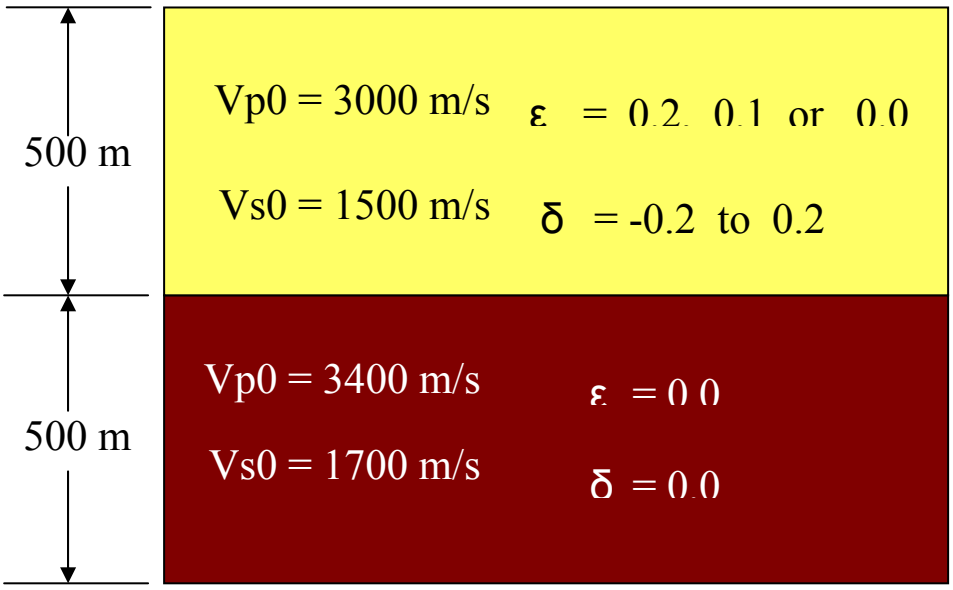

Figure 4.1 Model parameters

The anisotropy parameter ranges in our models (Figure 4.1) cover almost 80% of the anisotropy measured in sedimentary rocks. We can see from the measurements made by Thomsen in 1986 (Figure 4.2) that δ goes from -0.2 to 0.2, and ε goes from 0.0 to 0.2.

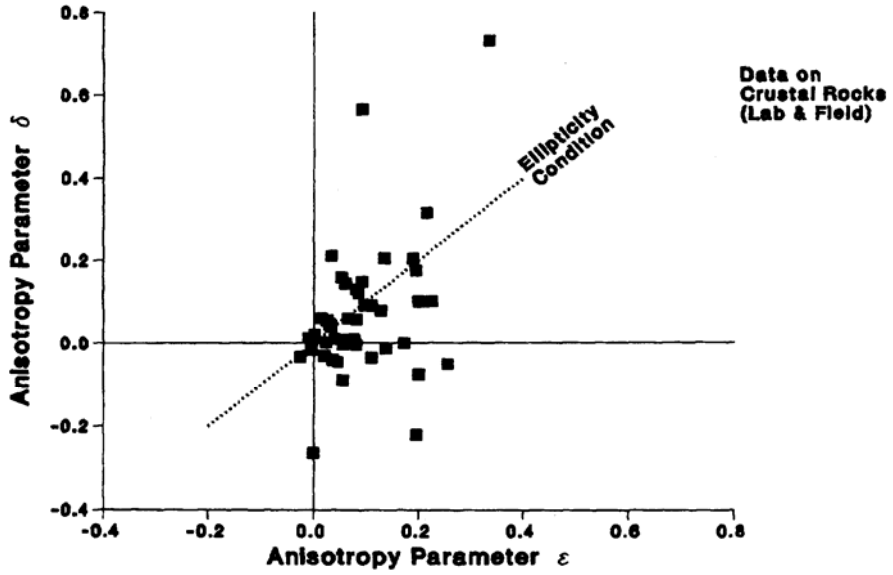

Figure 4.2 This figure indicates the noncorrelation of the two anisotropy parameters δ and ε for the measured anisotropy in sedimentary rocks. (Thomson, 1986)

Using Equations (3.33), (3.34), (3.35) and (3.36), we can pick up effective coefficients A_2, A_4, V_{NMO}, V_{h} and S, and then obtain anisotropy parameters ε and δ by using Equations (3.37), (3.38), and (3.39) through a Dix-type differentiation procedure (here, vertical P-wave velocity α_0 is known from a well log, check shot, or VSP). Semblance scanning is employed to estimate effective coefficients.

4.1.1 Estimation of Thomsen's anisotropy parameters versus offset range

Our estimation has been performed on short offset, mid-offset and long-offset, respectively. Figure 4.3 shows reflection-traveltime approximations to true reflection traveltime at the offset range *x/z* = 0.5, 1.0, 1.5 and 2.0. It can be seen from Figure 4.3 that within its own offset range, the accuracy of estimated delta decreases with offset. Our research also shows that the accuracy of estimated epsilon increases with offset. This also means within their own offset range, delta should be estimated over the short offset and epsilon should be estimated over the long offset. So we will estimate delta at offset/depth = 1.0, and estimate epsilon at *x/z* = 2.0.

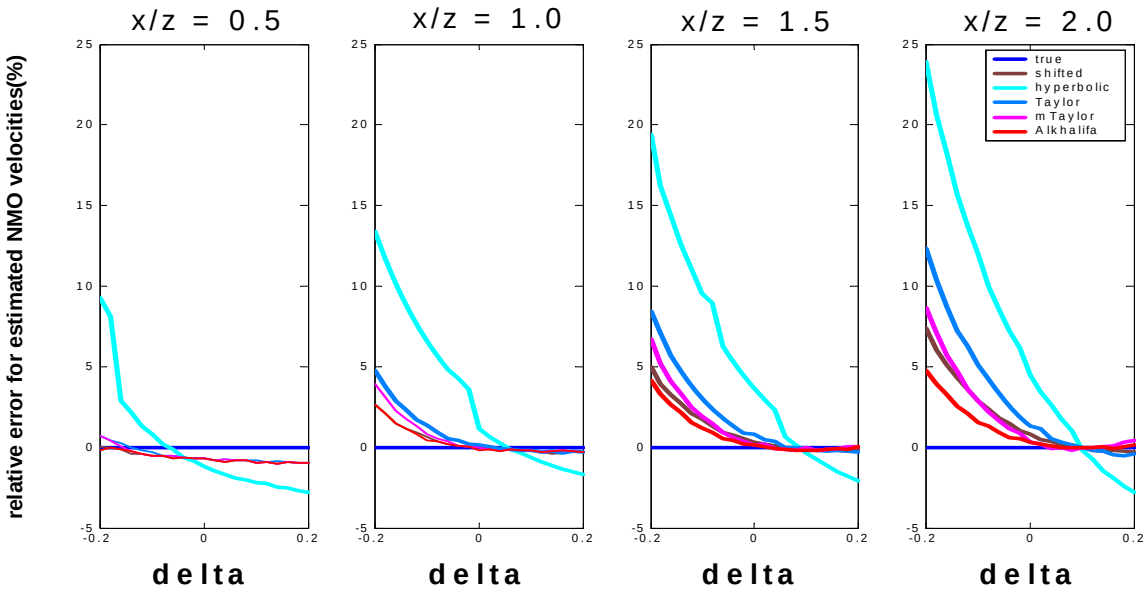

Figure 4.3 Reflection-traveltime approximations to true reflection traveltime within different offset ranges.

4.1.2 Estimation of Thomsen's anisotropy parameters versus model anisotropy parameters

Figure 4.4 shows the errors in estimated δ, plotted versus true δ when offset/depth = 1.0, for ε values of 0.2, 0.1 and 0.0, and δ values ranging from –0.2 to 0.2 in increments of 0.02. From Figure 4.4 it appears that i) the smaller the value of $(\varepsilon - \delta)$, the higher the

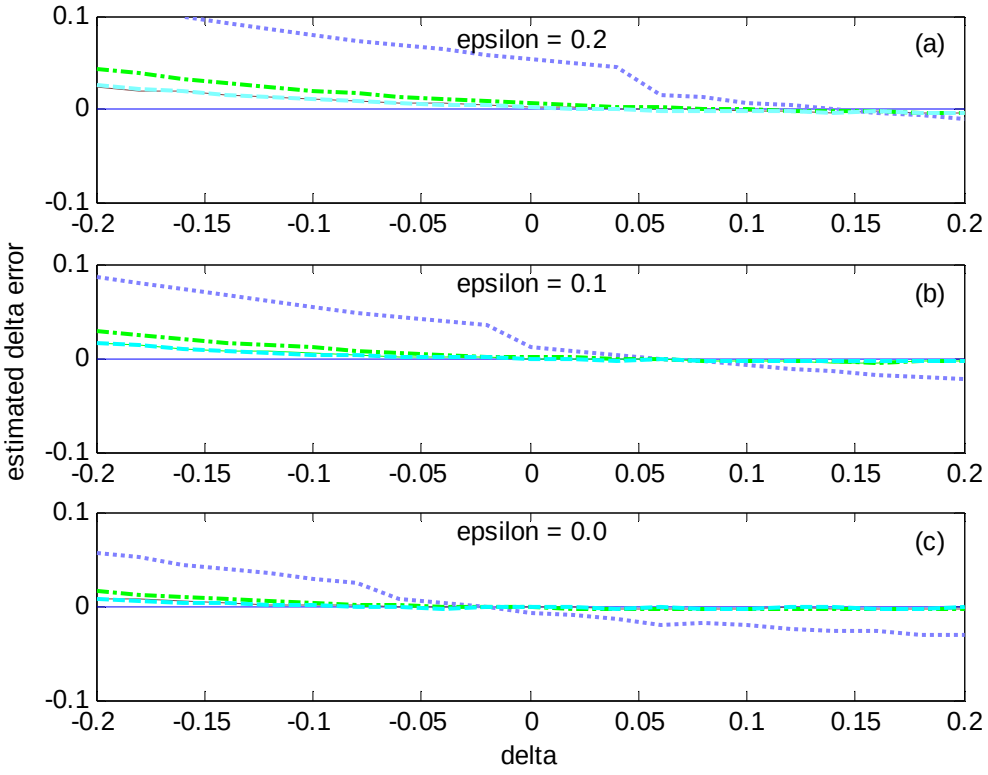

Figure 4.4 The error in estimated δ plotted vs. true δ for various values of ε, for offset/depth = 1.0. Blue solid line: the exact anisotropy parameters; purple dotted line: hyperbolic traveltime inversion; green dash-dot line: the modified three-term Taylor-series inversion; red solid line: the shifted hyperbolic inversion; cyan dashed line: Alkhalifah's inversion.

accuracy of the estimated δ value; ii) the estimated values deviate greatly from the true values when $|\varepsilon - \delta| > 0.2$, and iii) the Alkhalifah's and the shifted-hyperbolic estimations are better than the modified three-term Taylor-series method, which in turn is better than hyperbolic estimation.

Figure 4.5 shows the errors in estimated ε, plotted versus true δ when offset/depth = 2.0, for ε values of 0.2, 0.1 and 0.0, and δ values ranging from –0.2 to 0.2 in increments of 0.02. From Figure 4.5 we can see that only Alkhalifah's inversion is able to estimate parameters ε with certain accuracy.

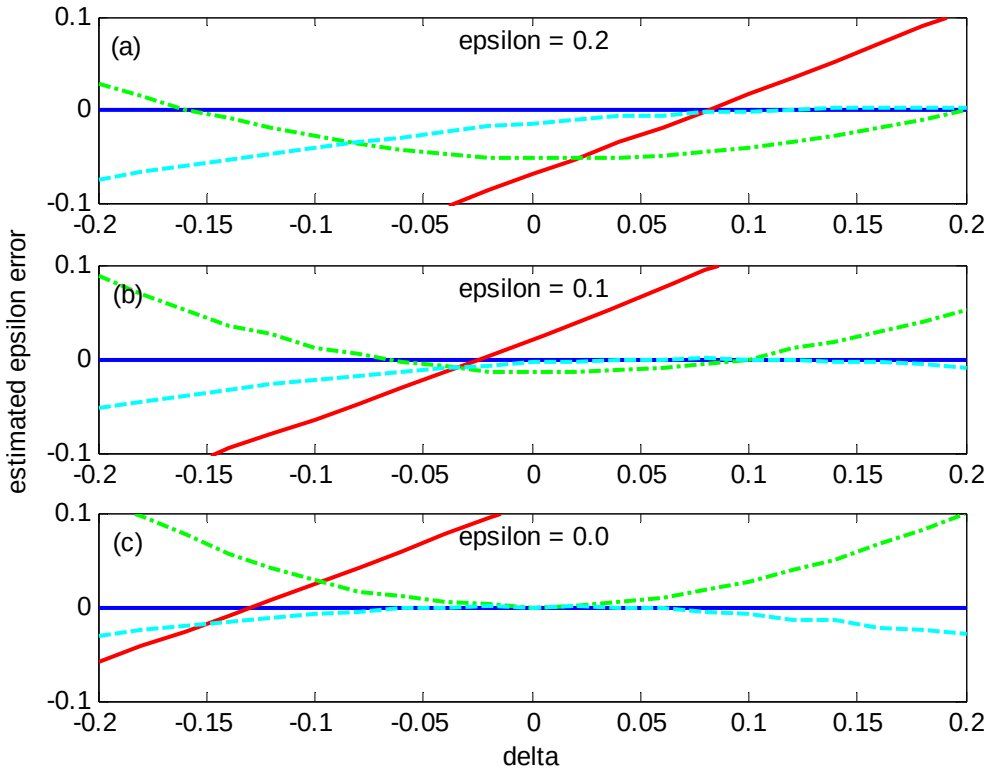

Figure 4.5 The error in estimated ε plotted vs. true δ when offset/depth = 2.0. Green dash-dot line: the modified three-term Taylor-series inversion; red solid line: the shifted hyperbolic inversion; cyan dashed line: Alkhalifah's inversion.

4.2. Layered VTI media

Table 4.1 demonstrates the model parameters for a four-layer model. Note that all ($\varepsilon - \delta$) values in model I are less than 0.2. The only difference between model II and model I is that the value of ($\varepsilon - \delta$) in the second layer is larger than 0.2.

Table 4.1 Model parameters for layered VTI media

Thickness (m)	Time interval (ms)	α_0 (m/s)	β_0 (m/s)	Model I ε , δ	Model II ε , δ
500	357	2800	1400	0.20, 0.10	0.20, 0.10
500	333	3000	1500	0.15, 0.08	0.20, - 0.20
500	312	3200	1600	0.10, 0.04	0.10, 0.04
500	285	3500	1750	0.08, 0.02	0.08, 0.02

Figure 4.6 shows estimated anisotropy-parameter values (dashed lines) by using Alkhalifah's methods and actual values (solid lines). These estimation results from multilayer VTI media also demonstrate that the estimated interval anisotropy parameters are very close to the true parameter values. Only when ($\varepsilon - \delta$) is larger than 0.2 do the estimated interval parameter values depart significantly from the true value.

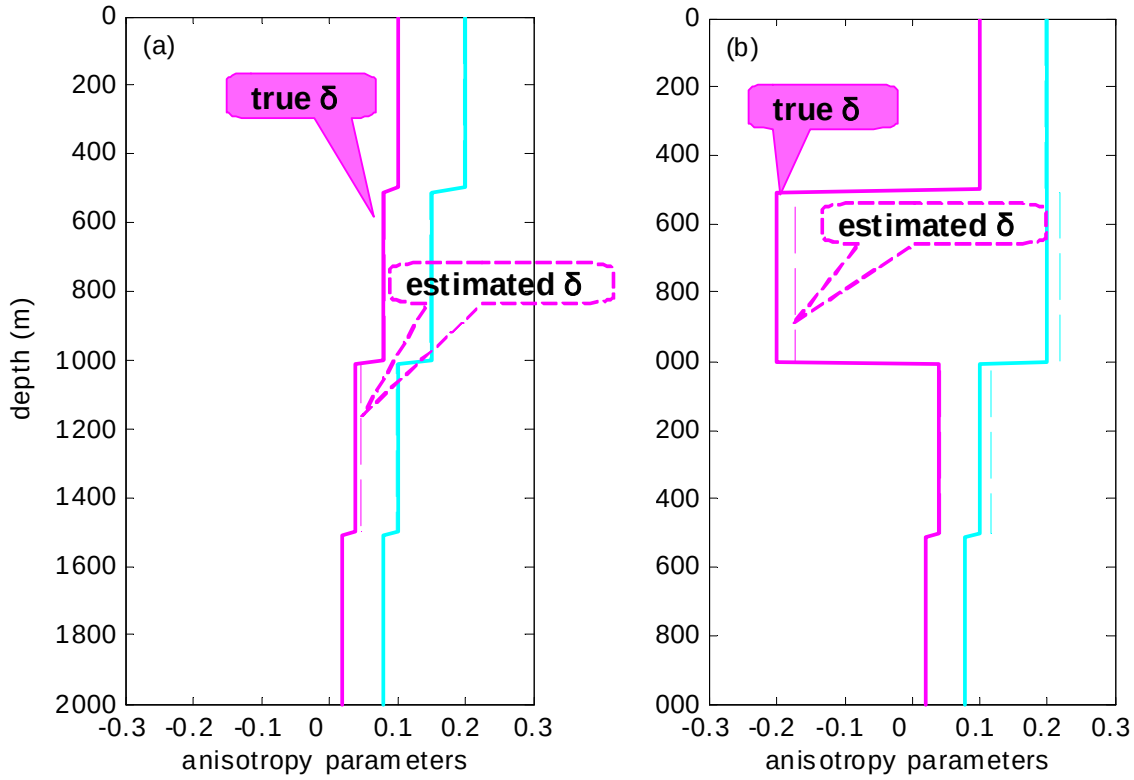

(a) (b)

Figure 4.6 Estimated anisotropy parameters δ (dashed magenta line) and ε (dashed cyan line); and true parameters δ (solid magenta line) and ε (solid cyan line); (a) for Model I; (b) for Model II.

4.3. Conclusions

The accuracy of the estimated anisotropy parameter δ depends not only on the accuracy of the picked NMO velocity but also on the value of $(\varepsilon - \delta)$. The smaller the value of $(\varepsilon - \delta)$ and the value of ε, the higher the accuracy of estimated δ. The results of the four traveltime inversions by semblance analysis for the seismic examples demonstrate that the Alkhalifah's and shifted-hyperbolic estimations are better than the modified three-term Taylor-series method, which in turn is better than hyperbolic

estimation. Only Alkhalifah's inversion can be used to estimate accurately the anisotropy parameter ε. Table 4.2 summarizes the relationships between the four methods and estimated anisotropy parameters

Table 4.2 The methods for estimating anisotropy parameters and their evaluation of estimated anisotropy parameters at short and long offsets

Methods	Moveout equations	Offset range	δ (short offset)	ε (long offset)
Hyperbolic	$t^2(x) = t_0^2 + \frac{x^2}{V_{\text{NMO}}^2}$	$x<z$	bad,	bad
Modified three-term Taylor	$t^2(x) = t_0^2 + \frac{x^2}{V_{\text{NMO}}^2} + \frac{A_4 x^4}{1+\left(\frac{x}{\alpha_0 t_0}\right)^2}$	$z<x<1.0z$	good,	bad
The shifted hyperbolic	$(t_{\text{sh}} - \tau_s)^2 = (t_0 - \tau_s)^2 + \frac{x^2}{V_{\text{sh}}^2}$	$z<x<1.5z$	good,	bad
Alkhalifah's (special case of three-term Taylor)	$t^2(x) = t_0^2 + \frac{x^2}{V_{\text{NMO}}^2} - \frac{\left(V_{\text{h}}^2 - V_{\text{NMO}}^2\right)x^4}{V_{\text{NMO}}^2\left(t_0^2 V_{\text{NMO}}^4 + V_{\text{h}}^2 x^2\right)}$	$z<x<2.0z$	best,	good

CHAPTER 5: APPLICATION TO BLACKFOOT SEISMIC DATA

We have demonstrated the viability of using the joint inversion of P-wave reflection traveltimes and well data to give Thomsen's anisotropy parameters, ε and δ, by applying it to synthetic data. However, the practical application of this approach to real data is a more challenging task. Firstly, application of the algorithm requires the recovery of nonhyperbolic moveouts from long-spread CMP gathers. Secondly, the semblance search at high incidence angles is also hindered by phase shifts in postcritical reflections. Thirdly, we have to consider the influence of noise on semblance. This chapter describes the application of the Alkhalifah's moveout velocity analysis technique to the real data from the 1997 Blackfoot survey.

5.1. Blackfoot seismic data processing

Processing seismic data for anisotropy parameter estimation is a challenge. Ideally, processing should improve the continuity and resolution of events to facilitate event identification and allow traveltime picks to the largest offset range possible (nonhyperbolic moveout is only evident in the far offset). We are only interested in traveltime moveout information; conservation of frequency content and amplitudes is less important.

Hence, the processing sequence employed starts with AGC, and bandpass filter. Two f-k filters are then applied to reduce the linear noise on the far offsets such that the picks can be extended to greater offsets. Then a surface-consistent predictive

deconvolution filter is designed to further reduce the linear noise and improve the lateral continuity of reflectors. A second bandpass filter is applied to remove high-frequency noise introduced by the predictive deconvolution filter. Finally, adjacent CMPs are combined and similar offsets stacked.

These steps improve the continuity of reflections significantly. An extensive series of tests was carried out to guarantee that the signal-to-noise ratio was improved and that events could be picked to large offsets without affecting the curvature of the reflections. Input data for the application of this method is raw data with static corrections applied.

Figure 5.1 shows a seismic line from south-central Alberta acquired by the CREWES Project in 1997. The line was processed with ProMAX seismic data-processing software using a sequence of conventional algorithms without taking anisotropy into account. The processing sequence (Yilmaz, 2001) to produce a post-stack migration is outlined below:

(1) SEG-Y seismic data input

(2) Preprocessing:

Setup of field geometry

Automatic gain control, bandpass filter

Editing (kills bad traces or reversed traces)

Picking first breaks for weathering statics calculation

Elevation correction

Weathering statics calculation (by GLI3D)

(3) Surface-consistent deconvolution and weathering statics correction

(4) CMP sorting and velocity analysis

(5) First residual statics correction and velocity analysis

(6) Second residual statics correction and velocity analysis

(7) NMO correction, muting and stacking

(8) Deconvolution

(9) Time-variant spectral whitening and filtering

(10) CDP trim statics

(11) Finite-difference migration

(12) SEG-Y output

Conventional velocity analysis was carried out along the line before the horizons were selected in order to avoid picking multiples and as a quality control on inversion results.

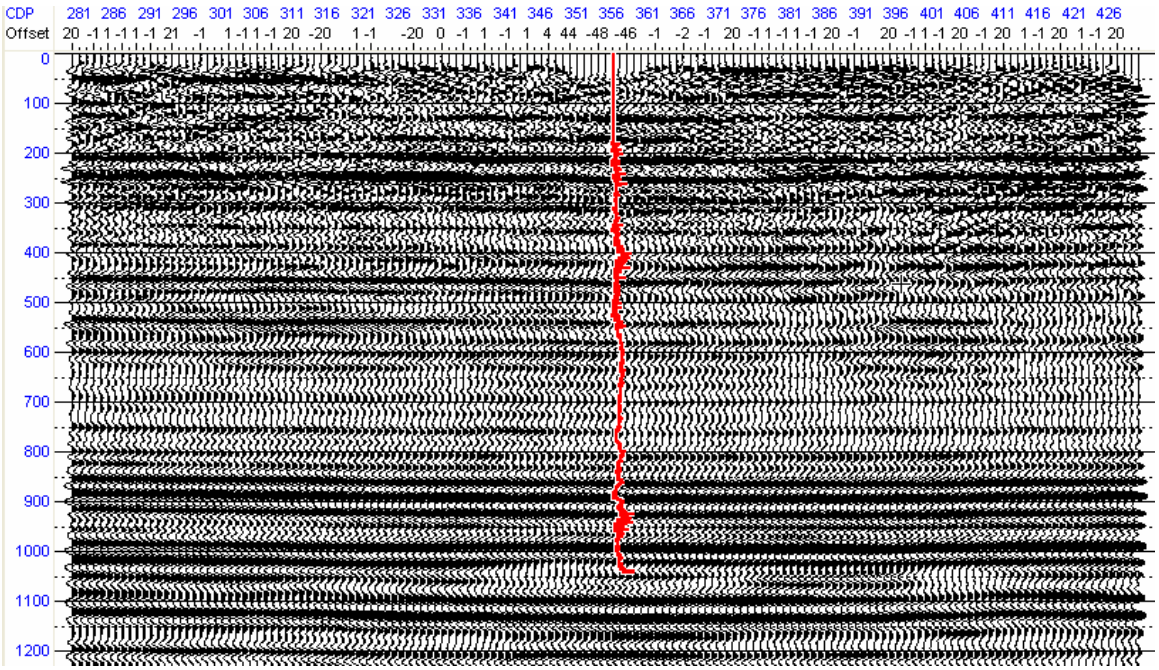

Figure 5.1 Post-stack migration using a sequence of conventional algorithms.

We selected CMP gather 357, in which location we have sonic log (the red curve in Figure 5.1), for anisotropy moveout velocity analysis. Figure 5.2(a) shows the correlation of well logs, synthetic data and Blackfoot seismic data as well as interpreted formation tops. The five seismic interfaces (including free surface) shown in Figure 5.2(b) are chosen for purposes of estimating Thomsen's anisotropy parameters. Figure 5.3 is the CDP gather for estimating effective coefficients. At zero offset, two-way reflection traveltimes of these four reflection events are t = 786, 868, 966,and 1022 ms and the depths of these four reflections are 1.2, 1.34, 1.52 and 1.63 km (see Figure 5.2). The far offsets of these reflections are about 2.8 km. So the offset ranges of these four reflection events are 3.17, 2.09, 1.31 and 1.72, respectively. The picking was done on the CMP shown in Figure 5.3 in which the offset is approximately twice depth of each event.

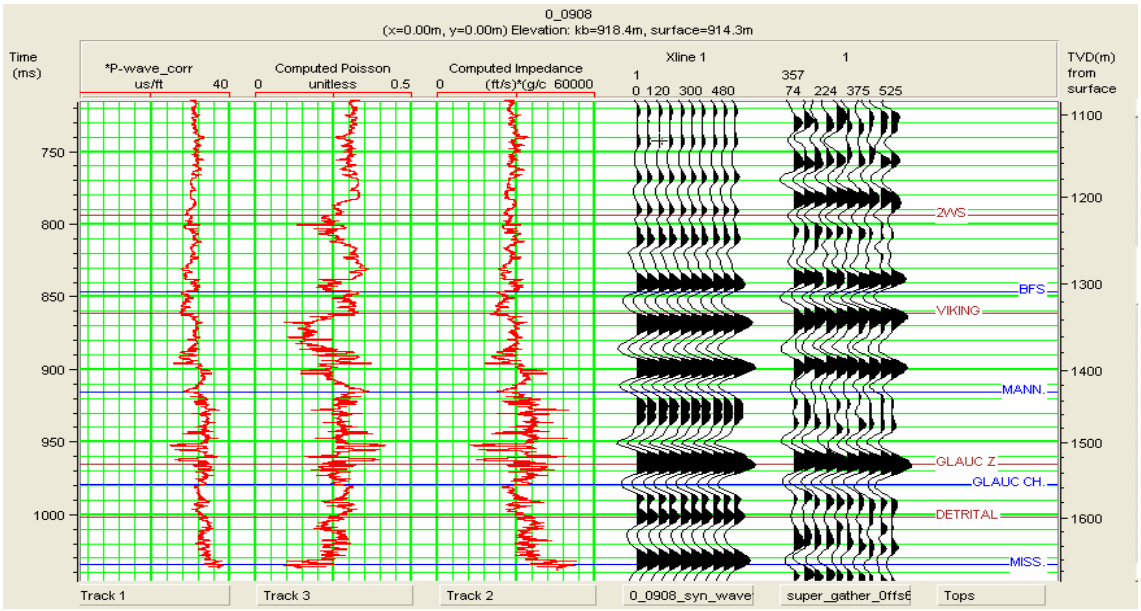

(a)

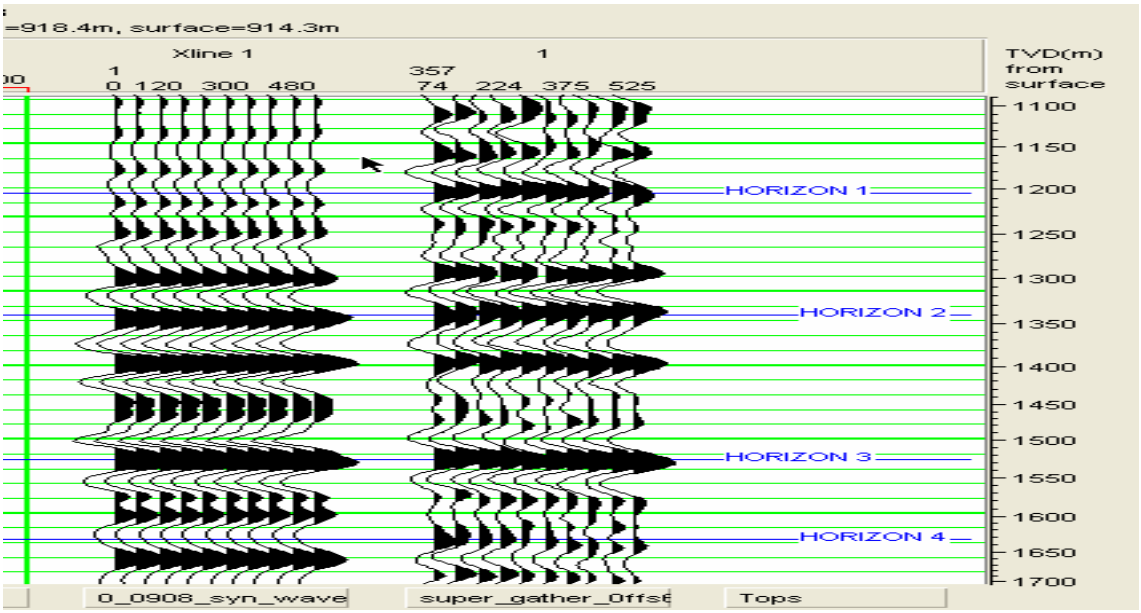

(b)

Figure 5.2 Correlation of synthetic data and real seismic data (a) with formation tops and (b) with the horizons.

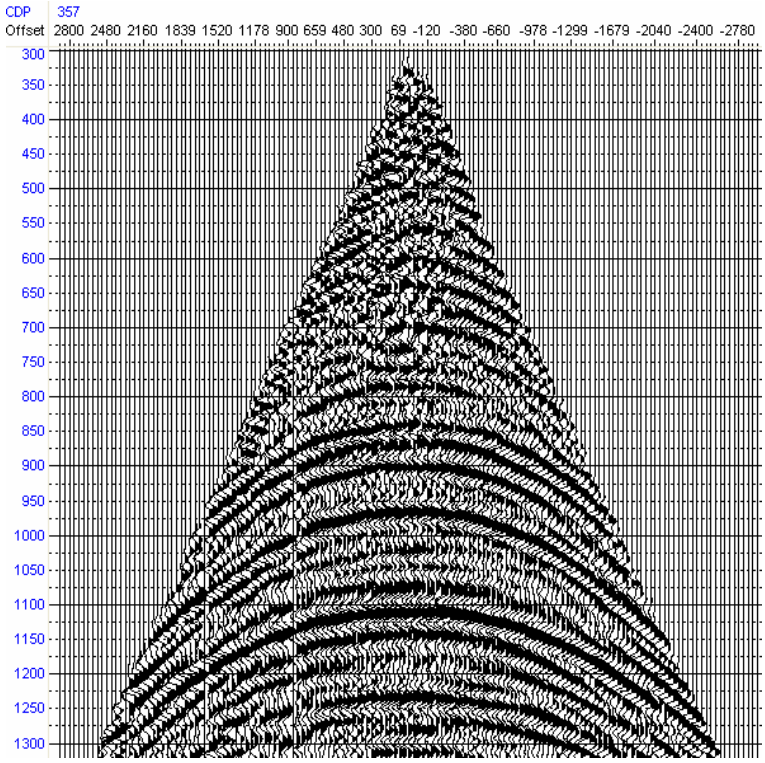

Figure 5.3 The CDP gather for estimating effective coefficients.

5.2. Interval vertical velocities from sonic log

Although anisotropy moveout (AMO) analysis can provide information about horizontal velocity, conventional moveout analysis using either NMO or AMO equations cannot provide information about vertical velocity (Yang et al., 2002). Obtaining vertical velocities was an important objective in our experiment.

Figure 5.4 shows the vertical interval velocities from sonic log which is located at the CMP gather of 357 (see Figure 5.1). The blue curve in Figure 5.4 was obtained from

P-wave sonic log (see the track 1 in Figure 5.2(a)). The red curve is the "blocky" velocities which have been used in estimating anisotropy parameters.

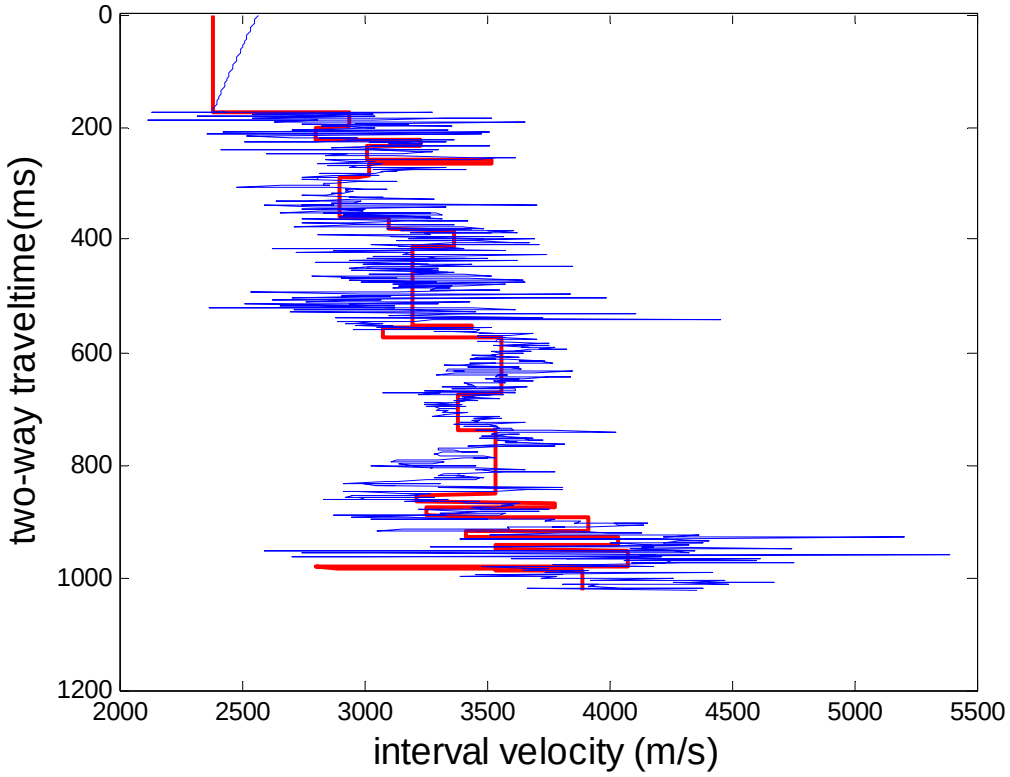

Figure 5.4 Vertical interval velocities from sonic well log data. Blue line before block and red line after block.

5.3. Estimation of Thomsen's anisotropy parameters

To obtain the best stack, we can make as many picks as necessary to honour changes in vertical velocity gradients. However, picks at short time intervals can yield anomalous interval coefficients from Dix-type differentiation (Yilmaz, 2001). For this reason, we should use picks at larger time intervals to estimate anisotropy parameters. From our experiments, the time interval (two-way time) should be greater than 200 ms.

Estimated values of moveout velocities and effective values of the anisotropy parameters, as well as the vertical interval velocities from sonic data, are shown in Tables 5.1 and 5.2. In Table 5.1, several of the estimated anisotropy parameters ε and δ in layers 2, 3 and 4 are unreasonable (larger than 0.5) due to time intervals being too small (less than 100 ms).

Estimated values ε of δ and in Table 5.2 seem more reasonable. The new layer 2 (from horizon 1 to horizon 4, our target zone) exhibits relatively high, but not unreasonably high, values of anisotropy. Layer 1 (above horizon 1) displays lower values of anisotropy.

Table 5.1 Estimated effective coefficients and anisotropy parameters (time interval < 200 ms)

Layer	Time interval(ms)	α_0 (m/s)	V_{NMO} (m/s)	V_h (m/s)	ε , δ
1	786	3099	2919	3185	0.0281, -0.0564
2	82	3299	3266	3257	0.5587, +0.9353
3	98	3823	3279	3637	0.6902, -0.1063
4	56	3882	3315	3782	0.3880, -0.0286

Table 5.2 Estimated effective coefficients and anisotropy parameters (time interval > 200 ms)

Layer	Time Interval(ms)	α_0 (m/s)	V_{NMO} (m/s)	V_h (m/s)	ε , δ
1	786	3099	2919	3185	0.0281, -0.0564
2	236	3882	3315	3782	0.3737, 0.2029

5.4. Interpretation and discussion

The presence of anisotropy causes two principal distortions in reflection moveouts. First, the short-spread moveout velocity in the presence of anisotropy is not, in general, equal to the RMS vertical velocity, even for horizontal layers (Thomsen, 1986). Thus, the application of the Dix formula in anisotropic formations results in erroneous interval velocities and inaccurate estimations of reflector depths.

Secondly, anisotropy leads to nonhyperbolic moveout, even in a homogeneous layer. If not properly corrected for, nonhyperbolic moveout causes distortions in velocity estimation and deteriorates the quality of stacked sections.

Ever since Dix's classic paper (1955), velocity analysis based on a hyperbolic moveout model has been widely used. Velocities estimated in this way are routinely used to improve signal quality by stacking multifold seismic data. However, as exploration interests turn to subtle stratigraphic traps associated with thin layers, the hyperbolic traveltime model is no longer adequate to preserve the signal resolution through stacking.

In conclusion, if the objective is to obtain a time-related seismic section, moveout-velocity analysis at selected CMP locations along the line yields a robust velocity section. If, on the other hand, the objective is to derive interval coefficients from Dix-type differentiation in order to obtain a depth-related seismic section, then the time interval should be larger than 200 ms to yield results that are geologically plausible.

CHAPTER 6: CONCLUSIONS

There are various methods for estimating anisotropy parameters, but no one perfect method. Each method has its own assumptions and limitations. The performance of each of the five reflection traveltime methods for estimating seismic anisotropy parameters in a VTI medium described and compared in Chapter 2, depends on the particular data example under consideration, and on how well a particular dataset fits the assumptions of each method. The choice of anisotropy parameter estimation method should be based on the knowledge of subsurface properties, geometry and wave mode of seismic data available and objectives for estimating anisotropy parameters.

Most methods for estimating Thomsen's anisotropy parameters are based on approximations of reflection coefficients and/or moveout velocities. Anisotropic moveout velocity analysis methods are based on moveout velocities which are used to estimate anisotropy parameters in a VTI medium in combination with well-log data. Analyses of four reflection-traveltime inversions (including hyperbolic, shifted hyperbolic, modified three-term Taylor series and Alkhalifah's in weakly anisotropic media) show that inversion accuracy is related to the spread length and subsurface anisotropy parameters.

When considering offset, the accuracy of estimated δ decreases with increasing offset while the accuracy of estimated ε increases with increasing offset. The accuracy of the estimated Thomsen anisotropy parameter δ depends not only on the accuracy of

the picked moveout velocity but also on the subsurface anisotropy parameters. The smaller the value of $(\varepsilon - \delta)$, the greater the accuracy of the estimated δ value.

The results of four reflection-traveltime inversions by semblance analysis for synthetic seismic examples demonstrate that in estimating δ, the Alkhalifah's and the shifted-hyperbolic estimations are better than the modified three-term Taylor-series method. Only the Alkhalifah's approximation can be used to estimate the anisotropy parameter ε with certain accuracy. Hyperbolic estimation is only suitable for estimating elliptical anisotropy.

A more challenging task is the practical application of anisotropic moveout velocity analysis methods. Our research shows that, if the objective is to derive interval coefficients from Dix-type differentiation, the time interval should be larger than 200 ms to yield results that are geologically plausible.

Accurate estimation of the velocity field is the most difficult step in imaging seismic data for anisotropic media. If anisotropy is applicable, then the methods described in this thesis provide a sound basis for improving larger volumes of data with, for example, reflection tomography.

REFERENCES

Alkhalifah, T., and Tsvankin, I., 1995, Velocity analysis for transversely isotropic media: Geophysics, **60**, 1550–1566.

Alkhalifah, T., 1997a, Velocity analysis using nonhyperbolic moveout in transversely isotropic media: Geophysics, **62**, 1839–1854.

Alkhalifah, T., 1997b, Seismic data processing in vertically inhomogeneous TI media: Geophysics, **62**, 662–675.

Alkhalifah, T., 1998, Acoustic approximations for processing in transversely isotropic media: Geophysics, **63**, 623–631.

Alkhalifah, T., and Larner, K., 1994, Migration errors in transversely isotropic media: Geophysics, **59**, 1405–1418.

Allen, J. L., and Peddy, C. P., 1993, Amplitude variation with offset: Gulf Coast case studies: Soc. Expl. Geophys.

Baan, M. V. D., and Kendall, J. M., 2002, Estimating anisotropy parameters and traveltimes in the tau-p domain: Geophysics, **67**, 1076–1086.

Banik, N. C., 1984, Velocity anisotropy of shales and depth estimation in the North Sea Basin: Geophysics, **49**, 1411–1419.

Brown, R. J., Lamoureux, M. P., Slawinski, M. A., and Slawinski, R. A., 2000, Direct traveltime inversion of VSP data for elliptical anisotropy in layered media: CREWES Research Report, **12**. 2–8.

Byun, B. S., and Corrigan, D, 1990, Seismic traveltime inversion for transverse isotropy: Geophysics, **55**,192–200.

Byun, B. S., Corrigan, D., and Gaiser, J. E., 1989, Anisotropic velocity analysis for lithology discrimination: Geophysics, **54**, 1564–1574.

Castle, R. J., 1994, A theory of normal moveout: Geophysics, **59**, 983–999.

Chang, C. H., and Gardner, G. H. F., 1993, Effects of vertically aligned fractures on reflection amplitudes, an amplitude-versus-offset study: 63rd Ann. Internat. Mtg., Soc. Expl. Geophys., Expanded Abstracts, 769–771.

Daley, P. F., 2001, Snell's law in transversely isotropic media: CREWES Research Report, **13**, 463–477.

Dix, C. H., 1955, Seismic velocities from surface measurements: Geophysics, **20**, 68–86.

Elapavuluri, P., and Bancroft, J. C., 2002, Estimation of Thomsen's anisotropy parameter δ and ε using EO gathers: CREWES Research Report, **14**, 1–14.

Gaiser, J. E., 1990, Transversely isotropic phase velocity analysis from slowness estimates: Journal of Geophysical Research, **95**, 11241–11254.

Grechka,V., and Tsvankin, I., 1998, Feasibility of nonhyperbolic moveout inversion in transversely isotropic media: Geophysics, **63**, 957–969.

Hake, H., 1986, Slant stacking and its significance for anisotropy: Geophys. Prospect, **34**, 595–608.

Hake, H., Helbig, K., and Mesdag, C. S., 1984, Three-term Taylor series for $t^2 - x^2$ curves over layered transversely isotropic ground: Geophys. Prospect, **32**, 828–850.

Isaac, J.H. and Lawton, D.C., 2004, A practical method for estimating effective parameters of anisotropy from reflection seismic data: Geophysics, **69**, 681–689.

Larner, K. L., 1993, Dip-moveout error in transversely isotropic media with linear velocity variation in depth: Geophysics, **58**, 1442–1453.

Leslie, J.M., and Lawton, D.C., 1998, A refraction seismic field study to determine the anisotropic parameters of shales: The Leading Edge, 17, 1127–1129.

Lou, M., Pham, L.D. and Willis, J. , 2002, Anisotropy parameter estimation from joint P- and C-wave data: SEG Expanded Abstracts, **21**, 1045.

Mallick, S., Craft, K.L., Meister, L.J. and Chambers, R.E., 1998, Determination of the principal directions of azimuthal anisotropy from P-wave seismic data: Geophysics, **63**, 692–706.

Miller, D. E., Leaney, S., and, Borland, W. H., 1994, An in situ estimation of anisotropic elastic moduli for a submarine shale: Journal of Geophysical Research, **99**, 21659–21665 .

Musgrave, M. J. P., 1970, Crystal acoustics: introduction to the study of elastic waves and vibrations in crystals.

Neidell, N.S. and Turhan Taner, 1971, Semblance and other coherency measures for multichannel data: Geophysics, **36**, 482–497.

Raymer, D. G., Kendall, J. and Beaudion, G. J., 1999, Measurements of salt anisotropy: Calculation Thomsen's δ parameter in real and synthetic data: SEG Expanded Abstracts, **18**, 1596.

Ruger, A., 1998, Variation of P-wave reflectivity with offset and azimuth in anisotropic media: Geophysics, **63**, 935.

Ruger, A., and Tsvankin, I., 1995, Azimuthal variation of AVO response for fractured reservoirs: 65th Ann. Internat. Mtg., Soc. Expl. Geophys., Expanded Abstracts, 1103– 1106.

Schmitt, D. R., and Kebaili, A., 1993, Velocity anisotropy estimation from slant stacks of wellbore seismics: Can. J. Expl. Geophys., **29**, 236–245.

Sena, A. G., 1991, Seismic traveltime equations for azimuthally anisotropic and isotropic media: Estimation of interval elastic properties: Geophysics, **56**, 2090-2101.

Seriff, A. J., and Sriram, K. P., 1991, P-SV reflection moveouts for transversely isotropic media with a vertical symmetry axis: Geophysics, **56**, 1271–1274.

Sexton, P. and Williamson, P., 1998, 3D anisotropic velocity estimation by model-based inversion of pre-stack traveltime: SEG Expanded Abstracts, **17**, 1855.

Taner, M. T., and Koehler, F., 1969, Velocity spectra-digital computer derivation and applications of velocity functions: Geophysics, **34**, 859–881.

Thomsen, L., 1986, Weak elastic anisotropy: Geophysics, **51**, 1954–1966.

Tsvankin, I., 1996, P-wave signatures and notation for transversely isotropic media: An overview: Geophysics, **61**, 467–483.

Tsvankin, I., and Thomsen, L., 1994, Nonhyperbolic reflection moveout in anisotropic media: Geophysics, **59**, 1290–1304.

Tsvankin, I., and Thomsen, L., 1995, Inversion of reflection traveltimes for transverse isotropy: Geophysics, **60**, 1095–1107.

Tsvankin, I., 1995, Normal moveout from dipping reflectors in anisotropic media: Geophysics, **60**, 268–284.

Tsvankin, I., 1997, Reflection moveout and parameter estimation for horizontal transverse isotropy: Geophysics, **62**, 614–629.

Vander Stoep, D. M., 1966, Velocity anisotropy measurements in wells: Geophysics, **31**, 900–916.

Vestrum, R. W., Lawton, D. C., and Schmid, R., 1999, Imaging structures below dipping TI media: Geophysics, **64**, 1239–1246.

Wang, Z., 2002a, Seismic anisotropy in sedimentary rocks, part 1: A single-plug laboratory method: Geophysics, **67**, 1415–1422.

Wang, Z., 2002b, Seismic anisotropy in sedimentary rocks, part 2: Laboratory data: Geophysics, **67**, 1423–1440.

Williamson, P., Sexton, P., Mispel, Joachim and Berthet, P., 1999, Anisotropic velocity model construction and migration: An example from West Africa: SEG Expanded Abstracts, **18**, 1592.

Winterstein, D. F., 1986, Anisotropy effects in P-wave and SH-wave stacking velocities contain information on lithology: Geophysics, **51**, 661–672.

White. J. E., Martineau-Nicoletis, L., and Monash, C., 1983, Measured anisotropy in Pierre shale: Geophys. Prosp., **31**, 709–723.

Yang, S., Shih, C.C., Banik, N.C., Chen, J., Schultz, G., and Banik, A., 2002, Application of vertical velocity analysis for a vertically transversely isotropic medium: SEG Expanded Abstracts, **21**, 129–132.

Yan, L. and Lines, L. R., 2001, Seismic imaging and velocity analysis for an Alberta Foothills seismic survey: Geophysics, **66**, 721–732.

Yilmaz, O., 2001, Seismic data analysis (Vol. 1). 312.

APPENDIX A: Shifted Hyperbola moveout equations

Figure A-1 shows a red non-hyperbolic curve that represents the offset traveltimes for a horizontally layered earth, a blue curve that is hyperbolic relative to the surface at $t = 0$, and a black curve that is hyperbolic relative to the dashed horizontal time at time $t = \tau_s$ that is referred to as a shifted hyperbolic curve. The normal moveout velocity at zero offset is V_{NMO}, and the source-receiver offset is x.

The hyperbolic curve

$$t_{\text{h}}^2 = t_0^2 + \frac{x^2}{V_{\text{NMO}}^2}$$

fits the curvature at x = 0, but only for a short offset. When we shift the t axis by a time τ_s, we get the shifted hyperbolic curve

$$\left(t_{\text{sh}} - \tau_s\right)^2 = \left(t_0 - \tau_s\right)^2 + \frac{x^2}{V_{\text{sh}}^2},$$

that also has the same curvature at x = 0, but has a better fit over more offset. The asymptotes of the shifted hyperbola will intersect at $x = 0$, and $t = \tau_s$.

Castle (1994) uses a S parameter

$$S = \frac{t_0}{t_0 - \tau_s} = \frac{t_0}{\tau_0},$$

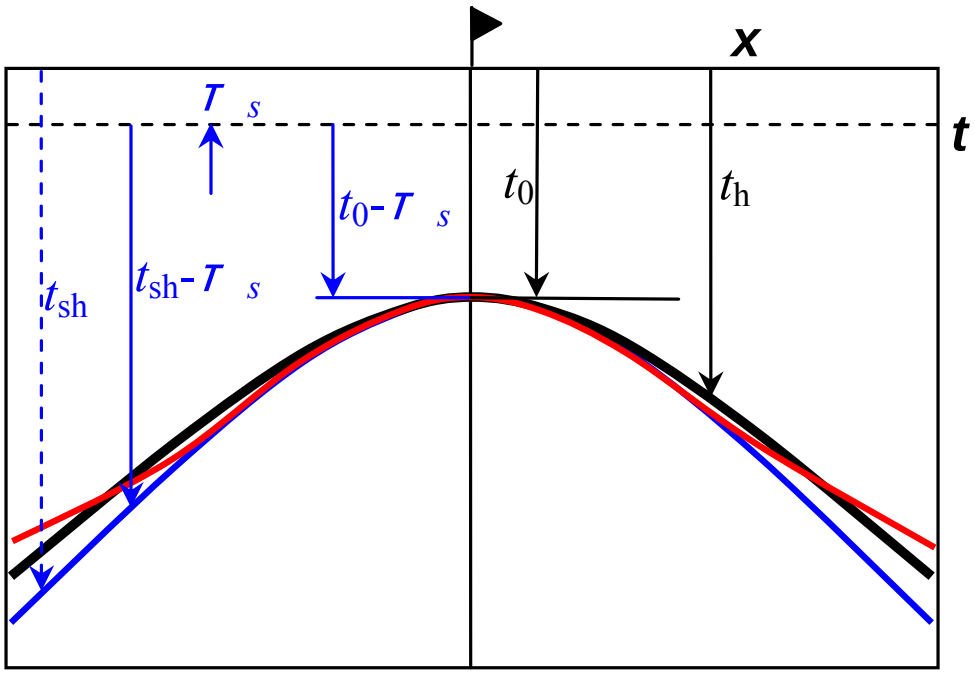

Figure A-1 Geometry of a hyperbolic NMO equation and the shifted hyperbola NMO equation. (After Bancroft, private communication)

to get a more common form of the shifted hyperbolic equation

$$t = t_0(1-\frac{1}{S}) + \sqrt{\left(\frac{t_0}{S}\right)^2 + \frac{x^2}{SV_{\text{NMO}}^2}}\,.$$

where we now have a change in the moveout velocity to $V_{\text{SH}}^2 = SV_{\text{NMO}}^2$. This represents a slight change in curvature at zero offset for the two hyperbolic curves.

We compute the new shifted hyperbola velocity from the curvature of the two moveout equations at zero offset. For the normal moveout hyperbola,

$$t_{\text{h}}^2 = t_0^2 + \frac{x^2}{V_{\text{NMO}}^2}$$

taking the first derivative,

$$\frac{2t_{\mathrm{h}}dt_{\mathrm{h}}}{dx}=\frac{2x}{V_{\mathrm{NMO}}^2},$$

then the second, we get

$$\frac{2t_{\mathrm{h}}d^2t_{\mathrm{h}}}{dx^2}+2\left(\frac{dt_{\mathrm{h}}}{dx}\right)^2=\frac{2}{V_{\mathrm{NMO}}^2}.$$

At zero offset

$$\frac{d^2t_{\mathrm{h}}}{dx^2}=\frac{1}{t_0V_{\mathrm{NMO}}^2}.$$

For the shifted hyperbola case,

$$(t_{\mathrm{sh}}-\tau_s)^2=(t_0-\tau_s)^2+\frac{x^2}{V_{\mathrm{sh}}^2},$$

the first derivative is

$$2(t_{\mathrm{sh}}-\tau_s)\frac{t_{\mathrm{h}}dt_{\mathrm{h}}}{dx}=\frac{2x}{V_{\mathrm{sh}}^2},$$

the second derivative is

$$2(t_{\mathrm{sh}}-\tau_s)\frac{d^2t_{\mathrm{sh}}}{dx^2}+2\left(\frac{dt_{\mathrm{sh}}}{dx}\right)^2=\frac{2}{V_{\mathrm{sh}}^2}.$$

At zero offset,

$$\frac{d^2t_{\mathrm{sh}}}{dx^2}=\frac{1}{(t_0-\tau_s)V_{\mathrm{sh}}^2}.$$

Since the two curvatures are the same at $x=0$, then

$$\frac{1}{t_0V_{\mathrm{NMO}}^2}=\frac{1}{(t_0-\tau_s)V_{\mathrm{sh}}^2},$$

or

$$V_{\text{sh}}^2 = \frac{t_0 V_{\text{NMO}}^2}{(t_0 - \tau_s)} = S V_{\text{NMO}}^2 ,$$

giving us a definition for the moveout velocity for the shifted hyperbolic equation.

Castle, J. C., 1994, A theory of normal moveout, Geophysics, Vol. 59, No.6, p 983-999.